

# **Thermal comparison of mono-facial and bi-facial photovoltaic cells considering the effect of TPT layer absorptivity**

Ali Radwan<sup>1,2</sup>, Montaser Mahmoud<sup>1,3</sup>, Abdul-Ghani Olabi<sup>1,4\*</sup>, Ahmed Rezk<sup>5</sup>, Hussein M  
Maghrabie<sup>6</sup>, Mohammad Ali Abdelkareem<sup>1,7\*</sup>

<sup>1</sup>Sustainable Energy & Power Systems Research Centre, RISE, University of Sharjah, P.O. Box 27272, Sharjah,  
United Arab Emirates

<sup>2</sup>Mechanical Power Engineering Department, Faculty of Engineering, Mansoura University, Mansoura 35516, Egypt

<sup>3</sup>Department of Engineering, School of Mathematics, Computer Science and Engineering, City, University of  
London, London, UK

<sup>4</sup>Mechanical Engineering and Design, Aston University, School of Engineering and Applied Science, Aston  
Triangle, Birmingham, B4 7ET, UK

<sup>5</sup>Energy and Bioproducts Research Institute (EBRI), College of Engineering and Physical Science, Aston  
University, Birmingham B4 7ET, UK

<sup>6</sup>Department of Mechanical Engineering, Faculty of Engineering, South Valley University, Qena 83521, Egypt

<sup>7</sup>Chemical Engineering Department, Minia University, Elminia, Egypt

## **Abstract**

With the widespread utilization of solar photovoltaics (PV), it is becoming increasingly important to understand its performance using various configurations to harvest solar energy at the most suitable efficiency, specifically in hot climates. Therefore, this paper compares mono-facial and bi-facial PV cells under the high-temperature desert climate of Sharjah (United Arab Emirates). The optimally tilted and vertical east-west configurations were compared to determine the best orientation for the studied conditions. In addition, new parameter, the rear side layer absorptivity of the mono-facial PV cell, was investigated. The comparative study considered solar radiation, ambient temperature, wind speed, and albedo. The results showed that considering the effect of

absorptivity achieves better performance predictions. However, the effect of the absorptivity did not exhibit a significant influence compared to the case with zero absorptivity. As such, the PV cell temperature increased by 0.4°C and 1.4°C at an albedo of 0.2 and 0.7, considering the actual absorptivity value (0.2). On the other hand, it is worth mentioning that improper designs result in considerable temperature rises as the absorptivity value increases. Under the investigated conditions and based on the year-long comparison, the tilted bi-facial performed better than the vertical bi-facial; as the albedo increased from 0.2 to 0.7, the power gain ratio of tilted bi-facial increased from 7.18% to 20.88% and that of vertical bi-facial from -19.4% to 12.65%.

**Keywords:** photovoltaic, mono-facial, bi-facial, thermal modelling, efficiency.

<b>Nomenclature</b>	
$c_p$	specific heat (J/kg.K)
$G$	solar radiation (W/m <sup>2</sup> )
$H$	time from local solar noon (hour)
$h$	convection heat transfer coefficient (W/m <sup>2</sup> .K)
$I$	incident solar radiation (W/m <sup>2</sup> )
$k$	thermal conductivity (W/m.K)
$L$	latitude angle
$N$	day number
$P$	power (W)
$P$	power (W)
$q$	heat generation (W/m <sup>3</sup> )
$r$	radiation (W/m <sup>2</sup> )
$T$	temperature (°C)
$t$	time (s)
$V$	speed (m/s)
$Z$	azimuth angle
<i>Greek letters</i>	
$\alpha$	solar latitude angle
$\beta$	surface tilt angle
$\delta$	declination angle

$\omega$	hour angle
$\eta$	efficiency (%)
$\theta$	angle of incidence
$\rho$	reflectivity
$\tau$	transmissivity
$\varphi$	zenith angle
<i>Abbreviations</i>	
ASHRAE	American Society of Heating, Refrigerating, and Air-Conditioning Engineers
AST	apparent solar time
Bf	bi-facial
DS	daylight saving
ESS	energy storage systems
ET	equation of time
EVA	ethylene vinyl acetate
GR	gain ratio
LL	local longitude
LST	local standard time
Mf	mono-facial
NREL	National Renewable Energy Laboratory
PV	photovoltaic
RES	renewable energy sources
SL	standard longitude
TPT	Tedlar Polyester Tedlar
<i>Subscripts</i>	
<i>amb</i>	ambient
<i>b</i>	beam
<i>bN</i>	normal beam
<i>d</i>	diffuse
<i>g</i>	ground
<i>H</i>	horizontal surface
<i>r</i>	reflected
<i>ref</i>	reference
<i>s</i>	surface
<i>sc</i>	solar cell
<i>sr</i>	sunrise
<i>ss</i>	sunset

$w$	wind
-----	------

## 1. Introduction

The growth of electricity demand is a major factor that affects climate change due to the dependency on fossil fuels for power generation. This elevates the importance of utilizing renewable energy sources (RES) such as solar [1], wind [2], geothermal [3], bioenergy [4], wave [5], tidal [6], and hydro [7] to supersede or retrofit the existing fossil-based power systems. RES-based power generation systems have a considerably lower impact on the environment than conventional systems [8]. Additionally, the low operating cost of most RES systems promotes the widespread of such systems and their economic feasibility.

Solar energy is one of the most utilized RES since it can be used in a wide variety of applications, including power generation [9], heating [10], cooling [11], ventilation [12], cooking [13], drying [14], and desalination [15]. Accordingly, solar energy has significantly contributed to several sustainable development goals (SDGs), such as SDG-6 (clean water and sanitation) SDG-7 (clean energy), SDG-11 (sustainable cities and environment), and SDG-13 (climate action) [16]. However, the stochastic and intermittent nature of solar energy is a significant challenge to the reliability and performance of the system. Therefore, integrating solar energy into hybrid energy systems is usually recommended so that the supplementary source can provide power during the night and cloudy hours [17]. Another approach can be the use of energy storage systems (ESSs), which can reduce power fluctuations, provide power during off-periods, and shave peak loads [18]. Solar energy has been coupled with many types of ESSs, such as compressed air [19], pumped hydro [20], batteries [21], phase change materials [22], hydrogen [23], supercapacitors [24].

One of the most valuable innovations in solar energy systems is the development of bi-facial photovoltaic (PV) cells. Their performance is generally higher than mono-facial cells as they can absorb solar radiation from both sides, which increases the amount of electricity produced. Several researchers investigated the effect of influential parameters and compared the performance of mono-facial and bi-facial PV cells. Zhang *et al.* [25] developed a model to study the influence of the incidence angle on the front and rear sides of bi-facial PV modules. A comparison of bi-facial and polycrystalline PV modules was carried out by Hariharasudhan *et al.* [26], considering the effect of partial shading. The results showed that the average loss in bi-facial PV is lower than that of polycrystalline PV by 26%. The effect of passive and active cooling on the performance of mono-facial and bi-facial floating PV plants was investigated by Tina *et al.* [27]. It was reported that passive cooling increases the energy collected from bi- and mono-facial PVs by 3% and 2.6%, respectively, while active cooling increases it by 9.7% and 9.5%. Gu *et al.* [28] reported that the energy gain of bi-facial PV increases at low solar radiation compared to that of mono-facial. This was noticed from the energy gain on sunny and cloudy days, which was 13.08% and 16.54%, respectively. This may be verified by the significant effect of solar radiation on the bi-facial PV cell temperature.

Bi-facial PV modules also performed better than mono-facial PV modules in building integrated systems. For example, Tina *et al.* [29] reported that bi-facial PV could increase the energy yield by 5% based on the weather conditions in Catania, Italy. M. Prasad and R. Prasad [30] also compared the bi-facial and mono-facial grid-connected solar farms based on a techno-economic analysis. The PVsys computational tool was employed to create and simulate the outcomes using historical weather data spanning 17 years and other grid and solar PV requirements. The results

indicated that the grid-connected bi-facial solar farm is preferable since it has a greater energy potential, a higher performance ratio, a greater potential for reducing greenhouse gas emissions, and a lower levelized cost of electricity. When compared to the mono-facial, it can also provide a more affordable alternative for grid-integrated solar PV while requiring less space, which is limited on small islands.

In [31], a comparison was made between mono-facial and bi-facial PVs' performances considering the effect of climate change. Based on the expected climatic conditions for 2050 and 2080, bi-facial PV delivered greater power production and was better in terms of climate change implications than mono-facial PV. On an hourly basis, the bi-facial PV showed an 18%–48% greater energy production than the mono-facial PV. Since the bi-facial panel's cell was transparent on both sides, its temperature was least influenced during the investigated period (2020-2080). According to their results, bi-facial PV's daily average energy yield was around 30% greater than that of mono-facial PV. Soulemane *et al.* [32] examined snow effects on the mono-facial and bi-facial PV systems in a wintery northern region. According to the findings, mono-facial snow losses are 33% on average during the winter and 16% annually. However, bi-facial systems operated more efficiently in harsh winter conditions than mono-facial ones, with average winter snow losses of 16% and worst-case yearly losses of 2%. Additionally, the bi-facial system gained 19% throughout the winter compared to the mono-facial system.

In seven locations around Brazil, Barbosa de Melo *et al.* [33] computationally studied the results of a photovoltaic plant using mono-facial and bi-facial modules mounted on a fixed structure and solar trackers. According to the findings, depending on the weather and system setup, the bi-facial gain varied from 3.78% to 8.16%, and the tracker gain varied from 13.40% to 18.20%. The overall

benefit from using bi-facial modules and trackers ranged from 19.39% to 27.39%. Therefore, it is worth emphasizing the possibility of integrating these technologies to improve solar facilities' technical and financial sustainability.

The novelty of this study is presented in three main aspects. First, this study includes the effect of rear-side radiation absorption on the thermal behavior of the PV module. Second, this study proposes detailed thermal modeling of both mono-facial and bi-facial PV cells. This model was validated against various previously published models available in the literature. Finally, a one-year simulation is conducted to compare the annual energy gain from a 5 kW PV system using mono-facial and bi-facial PV modules under the same conditions (Sharjah – United Arab Emirates). Two installation methods, vertical and optimally tilted, were compared based on their annual energy production. Accordingly, the article is divided into five main sections, including the introduction. The next section presents the theoretical model and the difference between mono-facial and bi-facial PV cells. Section 3 shows the model validation regarding received solar radiation and PV cell temperature. The results and discussion are presented in section 4, where the effects of solar radiation, ambient temperature, wind speed, TPT layer absorptivity, and albedo are analyzed. Finally, the main outcomes and conclusions are summarized in section 5.

## **2. Theoretical model**

The main objective of this study is to evaluate the thermal performance of mono-facial and benchmark it against bi-facial PV modules operating under meteorological conditions of the selected site (Sharjah – United Arab Emirates). The ground reflection part has only a minor effect on the power and thermal characteristics of a typical mono-facial PV module. However, it

influences bi-facial modules' performance. The solar radiation incident on a tilted surface comprises the beam, the isotropic diffuse, and the ground-reflected part. The beam component is the direct solar radiation without being scattered or diffused due to the effects of clouds and dust. The clearness index significantly affects the diffuse component [34]. The solar irradiance received by tilted surfaces is a strong function of solar radiation components incident on the horizontal surface.

The methodology applied in this study consists of three main steps. First, the incident solar radiation on a horizontal surface in the selected site is evaluated on a particular day. Then, these data are used to evaluate the irradiance received by the front and rear surfaces of both mono-facial and bi-facial PV modules. Second, solar radiation values and other metrological conditions, including the ambient temperature and wind speed, are used to simulate both modules thermally. An in-house code was employed to evaluate the solar radiation on a horizontal and tilted surface. Third, the data is coupled with the ANSYS-Fluent simulation tool to evaluate the thermal behavior using the finite volume technique.

The model used to evaluate the hourly solar radiation on tilted surfaces starts with evaluating several solar angles [35]. The declination angle ( $\delta$ ) was estimated, which varies seasonally because of the earth's tilt on its rotation axis and the revolution of the earth around the sun. The earth's axis is tilted by  $23.45^\circ$ , but if the earth's rotation axis is not tilted, the declination would have been constant and always equal to  $0^\circ$ . The value of  $\delta$  varies plus or minus this value, reaching  $0^\circ$  on the fall and spring equinoxes. The value of  $\delta$ , in degrees, for any day of the year ( $N$ ), varies with the day number throughout the year. Accordingly, the declination angle can be estimated as follows:



$$\delta = 23.5 \sin \left[ \frac{360}{365} \times (284 + N) \right] \quad (1)$$

where  $N$  is the day number in the year (e.g., 1 January  $N = 1$ , 21 March  $N = 80$ , 21 June  $N = 172$ , 21 September  $N = 264$ , and 21 December  $N = 355$ ). The second angle is the hour angle ( $\omega$ ). It describes the rotation of the earth around its polar axis. The earth rotates one complete rotation ( $360^\circ$ ) every 24 hours, which is equivalent to  $15^\circ$  per hour. The hour angle equals zero at solar noon. Therefore, 15 degrees of longitude equals one hour, with the afternoon hours designated as positive. The hour angle is evaluated as follows:

$$\omega = (AST - 12) \times 15 \quad (2)$$

where AST is the apparent solar time, and at solar noon, AST equals 12. The value of  $\omega$  is positive after the solar noon and negative before the solar noon. For instance, the value of  $\omega$  is equal to  $-15^\circ$  and  $+15^\circ$  at AST of 11:00 AM and 1:00 PM, respectively. It is worth mentioning that the AST is different from the local clock time. The AST is estimated using the following correlation:

$$AST = LST + ET \pm 4(SL - LL) - DS \quad (3)$$

where LST is the local standard time, ET is the equation of time, which is evaluated as a function of  $N$  as shown in equation (4), SL is the standard longitude, LL is the local longitude, and DS is the daylight-saving time, which can be either zero or 60 min according to the country's energy policy. For instance, the USA and UK use a DS of 60 min, usually from the end of March to the end of October. Because the UAE does not adjust the clock for daylight saving time, the DS in the UAE is considered zero.

$$ET = 9.87 \sin \left( 2(N - 81) \frac{360}{364} \right) - 7.53 \cos \left( (N - 81) \frac{360}{364} \right) - 1.5 \sin \left( (N - 81) \frac{360}{364} \right) \quad (4)$$

After evaluating the declination angle and the hour angle, another geographical angle is needed in the calculations, which is the latitude angle. The latitude angle ( $L$ ) represents the position of the location with respect to the north or south of the equator. The value of  $L$  changes between  $0^\circ$  and  $+90^\circ$  for the northern hemisphere,  $0^\circ$  and  $-90^\circ$  for the southern hemisphere, and  $0^\circ$  at the equator.

The declination and latitude angles are used to evaluate the day length. The day length is an critical parameter for estimating the sunrise and sunset times. The day length is twice the sunset hour because solar noon happens in the middle of the sunrise and sunset hours. The day length changes through the year and equals 12 hours at the spring and fall equinoxes. The equation used to evaluate the day length is expressed as follows:

$$\text{day length} = \frac{2}{15} \times \cos^{-1}[-\tan(L) \times \tan(\delta)] \quad (5)$$

The sunset ( $H_{ss}$ ) and sunrise ( $H_{sr}$ ) times, in hours, are estimated from local solar noon as follows:

$$H_{ss} = -H_{sr} = \frac{1}{15} \cos^{-1}[-\tan(L)\tan(\delta)] \quad (6)$$

The global solar radiation on horizontal surfaces ( $I_H$ ) is experimentally measured for a specific location using a pyranometer. This device is used to measure the total radiation from all directions.

The value of  $I_H$  is evaluated using the following correlation:

$$I_H = I_b + I_d \quad (7)$$

where  $I_b$  and  $I_d$  are the beam or direct radiation component and the diffuse component on horizontal surfaces, respectively. The hourly diffuse component on a horizontal surface ( $I_d$ ) represents the portion of solar radiation that passes through the atmosphere and is scattered due to water vapor,

clouds, and dust particles. This component of solar radiation cannot be focused or concentrated. Therefore, mathematical models are commonly used to estimate this component. These models are summarized in detail in [35], including the simplified parametric model used in this study for its flexibility in coupling it with the CFD model.

$$I_H = I_{bN} \times \cos(\varphi) + I_d \quad (8)$$

$$I_{bN} = A \times \exp\left[\frac{-B}{\cos(\varphi)}\right] \quad (9)$$

$$I_d = C \times I_{bN} \quad (10)$$

where  $I_{bN}$  and  $\varphi$  are the normal beam solar radiation on horizontal surfaces and the zenith angle, respectively. The constants A, B, and C are given for different models in Table 1. Furthermore,  $\varphi$  is the complementary angle of the solar altitude angle ( $\alpha$ ). The zenith angle ( $\varphi$ ) represents the angle between the sun ray and the vertical. The zenith and altitude angles are functions of declination angle, hour angle, and location latitude.

$$\sin(\alpha) = \cos(\varphi) = \sin(L)\sin(\delta) + \cos(L)\cos(\delta)\cos(\omega) \quad (11)$$

The constants A, B, and C for different models are estimated based on the data given in Table 1. To evaluate the hourly direct radiation on a horizontal surface,  $I_b$  from the estimated  $I_{bN}$ , the following correlation can be used:

$$I_b = I_{bN} \cos(\theta_z) \quad (12)$$

The value of  $I_H$  is evaluated as the sum of  $I_b$  and  $I_d$ . The previous equations were used to determine the solar radiation on a horizontal surface. However, for a tilted surface, the components of the

solar radiation include the beam radiation, diffuse radiation, and ground-reflected radiation. These three components are functions of the surface tilt angle ( $\beta$ ) and the estimated radiation components on a horizontal surface. To evaluate the solar radiation on the front surface of the PV panel, the following equation is used:

$$I_{\beta,f} = \underbrace{I_{b\beta}}_{\text{beam tilted}} + \underbrace{I_{d\beta}}_{\text{diffuse tilted}} + \underbrace{I_r}_{\text{ground reflected}} \quad (13)$$

These components represent the beam radiation on a tilted surface, diffuse radiation on a tilted surface, and the ground reflected component on a tilted surface. The direct beam component incident on a tilted surface can be evaluated using the following model:

$$I_{b\beta} = r_b I_b \quad (14)$$

where  $r_b$  is the beam radiation tilt factor, which defines the ratio between the beam radiation received by a titled surface to the beam solar radiation received by a horizontal surface.

$$r_b \approx \frac{\cos(\theta)}{\cos(\varphi)} \quad (15)$$

where  $\theta$  is the angle of incidence, which represents the angle between the sun's rays and the normal to the surface. The angle of incidence was evaluated using the following relation:

$$\begin{aligned} \cos(\theta) = & \sin(L)\sin(\delta) \cos(\beta) - \cos(L)\sin(\delta) \sin(\beta)\cos(Z_s) \\ & + \cos(L)\cos(\delta) \cos(\omega)\cos(\beta) + \sin(L)\cos(\delta) \cos(\omega)\sin(\beta) \cos(Z_s) \\ & + \cos(\delta)\sin(\omega) \sin(\beta)\sin(Z_s) \end{aligned} \quad (16)$$

where  $Z_s$  is the surface azimuth angle, which is the angle between the projection of the normal to the surface on the ground and the south direction. This angle is taken to be equal to zero for the

south-facing tilted surface of this study. Also, the optimal tilt angle is taken to be equal to the location latitude of Sharjah, UAE (25.3462° N, 55.4211° E).

Table 1: The values of constants A, B, and C used in the parametric model obtained from ASHRAE model given in [35].

	Jan.	Feb.	Mar.	Apr.	May	June	July	Aug.	Sep.	Oct.	Nov.	Dec.
<b>ASHRAE</b>												
<b>A</b>	1230	1215	1186	1136	1104	1088	1085	1107	1152	1193	1221	1234
<b>B</b>	0.142	0.144	0.156	0.18	0.196	0.205	0.207	0.201	0.177	0.16	0.149	0.142
<b>C</b>	0.058	0.06	0.071	0.097	0.121	0.134	0.136	0.122	0.092	0.073	0.063	0.057

The isotropic model is used to estimate the diffuse radiation on the tilted surfaces using Liu and Jordan's model, which is one of the simplest models of radiation and is presented as follows:

$$I_{d\beta} = \left[ \frac{1 + \cos(\beta)}{2} \right] \times I_d \quad (17)$$

The last component is the ground-reflected part ( $I_r$ ). This part is estimated using the following correlation:

$$I_r = \rho_g \times I_H \left[ \frac{1 - \cos(\beta)}{2} \right] \quad (18)$$

where  $\rho_g$  is the ground reflectivity. It is worth mentioning that both beam and diffuse radiation on a horizontal surface can be reflected on the front surface of the PV cell. Besides, the value of ground albedo changes throughout the day, measure by albedo meter, due to various factors, such as changes in ground properties with the passage of time, weather conditions, and the azimuthal distribution of homogeneities in the ground. In this study, it is assumed to be constant for simplicity. The albedo (from 0 to 1) represents the ratio between the diffuse reflection of solar radiation from the ground to the total incoming radiation. The minimal value (0) represents total absorption, and the maximum value (1) represents the total reflection. For instance, the albedo

values are around 0.25, 0.4, and 0.8 for green grass, dry desert sand, and clean snow ground, respectively. The albedo meter is made up of two identical Pyranometers that take measurements at the same time. One of these Pyranometers is facing upward and the other is facing downward to simultaneously measure the total received and ground-reflected radiations.

The above-mentioned equations can be used to evaluate the total radiation ( $I_{\beta}$ ) received by the frontal surface of the mono-facial PV cell and the bi-facial PV cell. However, the estimation of the rear side radiation is also important for the performance evaluation of the bi-facial PV module. Many models are available in the literature to estimate rear-side solar radiation [36-38]. In this study, we followed the method proposed by Durusoy *et al.* [34] for evaluating the rear-side irradiance. This model is the simplest and easiest for implementation with ANSYS-Fluent. They modified Liu and Jordan's isotropic diffuse model. First, for the rear side radiation, they replaced the value of  $\beta$  by  $(\pi-\beta)$  because the rear side is treated as the front side. The second modification is changing the value of  $R_b$ . All calculations are conducted for the period between the sunrise and the sunset. Negative values of  $R_b$ , on the front surface, have been taken as zero. The last modification is conducted for the ground reflected irradiation on the rear surface. They developed a model for the calculation of solar irradiation reaching the rear surface as follows:

$$I_{\beta,r} = \underbrace{R_{b,back} \times I_b}_{\text{beam on the rear}} + \underbrace{\left[ \frac{1 - \cos(\beta)}{2} \right] \times I_d}_{\text{diffuse on the rear}} + \underbrace{0.33 \left[ \frac{1 + \cos(\beta)}{2} \right] \times \rho_g \times I_H}_{\text{ground reflected on the rear}} \quad (19)$$

The thermal model calculation considers both estimated radiations on the front and rear sides. Figure 1 shows the schematic of the mono-facial and the bi-facial PV cells. The same construction of the bi-facial PV module in [39] and the mono-facial PV module in [40] was simulated. The

estimated hourly rear and front radiation received by the silicon wafer were used in the simulation. The simulation methodology starts with evaluating the internal heat generation in each layer of the PV module due to solar radiation absorption. This heat generation is taken as a source term in the energy equation of the solid layers as follows:

$$\rho_i c_{p,i} \left( \frac{\partial T}{\partial t} \right) = k_i \left( \frac{\partial^2 T}{\partial x^2} + \frac{\partial^2 T}{\partial y^2} + \frac{\partial^2 T}{\partial z^2} \right) + q_i \quad (20)$$

where  $T$ ,  $k_i$ , and  $q_i$  represent the temperature, layer thermal conductivity, and energy generation per unit volume, respectively. This equation is solved for every layer. The term  $q_i$  in the above equation changes according to each layer as presented in Table 2. More details about this technique can be found in the literature [40, 41].

Table 2: The heat generation absorption ( $\text{W}/\text{m}^3$ ) in each layer of the PV cell.

Layer	Mono-facial	Bi-facial
Front glass	$q_g = \frac{I_{\beta,f} \times \alpha_g}{\delta_g}$	$q_{g,1} = \frac{I_{\beta,f} \times \alpha_g}{\delta_g}$
Front EVA	$q_{eva} = \frac{I_f \times \tau_g \times \alpha_{eva}}{\delta_{eva}}$	$q_{eva,front} = \frac{I_{\beta,f} \times \tau_g \times \alpha_{eva}}{\delta_{eva}}$
Silicon wafer	$q_{sc} = \frac{(1 - \eta_{sc}) \cdot I_{\beta,f} \times \alpha_{sc} \times \tau_g \times \tau_{eva}}{\delta_{sc}}$ Where: $I_{\beta}$ is the total radiation on the front surface of a tilted surface	$q_{sc} = \frac{(1 - \eta_{sc}) \cdot I_t \times \alpha_{sc} \times \tau_g \times \tau_{eva}}{\delta_{sc}}$ Where: $I_t = I_{\beta,f} + I_{\beta,r}$
Rear EVA	$q_{eva,rear} = \text{zero}$ Assuming opaque cell where $\tau_{sc} = 0.04 \approx 0$ as in [40]	$q_{eva,rear} = \frac{I_{\beta,r} \times \tau_g \times \alpha_{eva}}{\delta_{eva}}$
Rear glass	No rear glass exists	$q_{g,rear} = \frac{I_{\beta,r} \times \alpha_g}{\delta_g}$
TPT layer	$q_{TPT} = \text{zero}$ Assuming opaque cell where $\tau_{sc} = 0.04 \approx 0$ as in [40]	No TPT layer exists

where  $\delta$ ,  $\alpha$ , and  $\tau$  are the layer thickness, absorptivity, and transmissivity, respectively. For the silicon wafer, the heat generation is considered a function of the solar cell efficiency as the net absorbed radiation is partially converted to heat and electricity in the silicon wafer. The electrical efficiency of the solar cell is evaluated using the following correlation as a function of cell temperature [36, 42]:

$$\eta_{sc} = \eta_{ref} \left( 1 - \beta_{ref} (T_{sc} - T_{ref}) \right) \quad (21)$$

where  $\eta_{ref}$  and  $T_{sc}$  are the PV efficiency at  $T_{ref}$  of 25°C and the temperatures of the solar cells, respectively. The value of  $\eta_{ref}$  used in this study is taken as 15% (AM1.5) at a reference temperature of  $T_{ref}$  with  $\beta_{ref}$  of 0.0045 K<sup>-1</sup> [42]. It is worth noting that the silicon wafer's heat generation value depends on the cell's unknown temperature. Therefore, an iterative approach is used. At low solar radiation levels as used in this study, less than 1000 W/m<sup>2</sup>, the second prediction shows a very close cell temperature to the third value as highlighted in [42, 43]. The instantaneous power generated by the PV cell per unit area is estimated using the following correlation:

$$P_{sc} = \alpha_{sc} \times \tau_g \times \tau_{eva} \times I_{total} \times \eta_{sc} \quad (22)$$

where  $I_{total}$  represents the total radiation received by the silicon wafer. In the mono-facial case, it takes the front radiation, while in the bi-facial PV cell, it is the sum of both rear and front radiation. Here it is worth mentioning that due to the existence of the electrical connection box on the rear side of the PV module, the received rear radiation from the rear side is multiplied by 0.9, which represents the percentage area covered by the cells on the rear side. The thermophysical properties of the solar cell layers are used as mentioned in [42] for mono-facial PV cells and as described in



[39] for bi-facial PV cells. The optical properties of each layer are used similarly to those presented in [42]. The mesh details for the mono-facial PV cell are depicted in Figure 1.

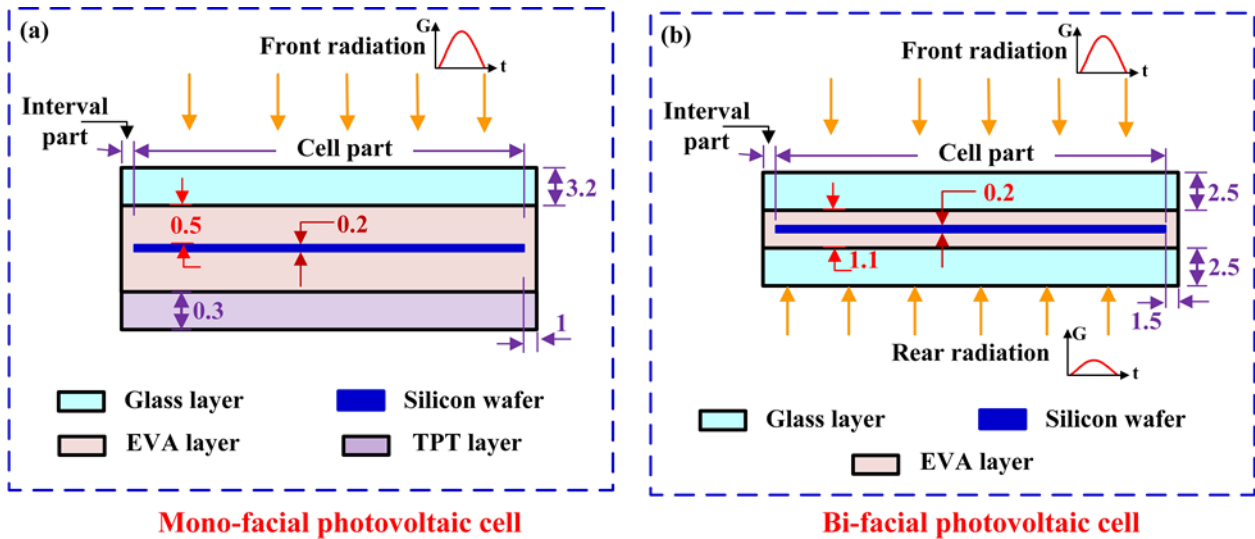
The boundary conditions applied in this study include mixed boundary conditions of convection and radiation heat loss from the front and rear surfaces of the simulated PV cell. In this case, the convection heat transfer coefficient at the front and rear sides is a function of wind speed. In addition, the front and rear surfaces' emissivity are defined with radiation temperatures equal to the ambient temperature. The back side heat transfer coefficient was equal to half of the front one due to the wind effect, as recommended by Zhou *et al.* [42]. The front convection heat transfer coefficient is evaluated using the following correlation:

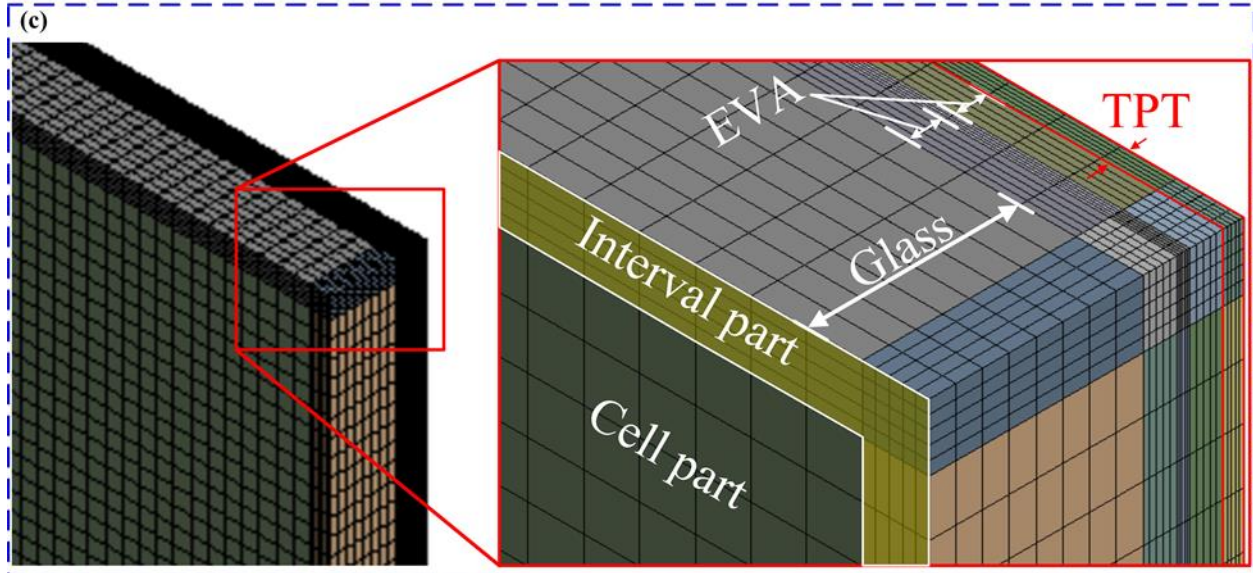
$$h_w = 5.7 + 3.8 \times U_w \quad (23)$$

Where  $U_w$  is the wind speed in m/s. The sides of the solar collector were assumed adiabatic because the module consists of multiple cells and the simulated cell can be considered a symmetrical domain. In addition, due to the very small thickness of the cell, this allowed adjusting this assumption as reported by Zhou *et al.* [42].

The detailed dimensions of the solar cell layers are used as mentioned in [42] for the mono-facial PV cell and in [39] for the bi-facial PV cell. The bi-facial PV cell consists of three materials: two glass layers covering the front and back faces; Ethylene Vinyl Acetate (EVA), a plastic filling located between the glasses; and lastly, the individual monocrystalline silicon cells. The silicon wafer, with a thickness of 0.2 mm, is embedded inside the EVA filling. Each of the two glasses is 2.5 mm thick [39]. The dimensions of the mono-facial PV cell include a glass cover, a silicon layer, an EVA layer, and a Tedlar Polyester Tedlar (TPT) layer. A tempered glass cover of 3.2 mm

thickness is used. In addition, a silicon wafer of 0.2 mm thickness is used in this PV panel. The silicon layer is embedded in the transparent encapsulation EVA layer with a thickness of 0.5 mm above, and below the silicon layer to fix it and provide both electrical isolation and moisture resistance. Furthermore, the TPT polymer layer is a photostable polyvinyl fluoride (PVF) layer with a thickness of 0.3 mm [42].





**Mesh details of the mono-facial PV cell**

Figure 1: Schematic of (a) mono-facial photovoltaic cell, (b) bi-facial photovoltaic cell, and (c) mesh details for the mono-facial PV cell as an example.

The computational domain is divided into multiple zones. This allows us to control the mesh, along with defining various source terms in every zone according to the light absorption. Figure 1c shows the details of the quadrilateral mesh used in the simulation. Various mesh tests have been performed at the beginning of the simulation to confirm that the results are independent of the mesh size. In more detail, as an example, the number of elements of 191012, 376832, 716800, and 1740248 are tested for the mono-facial PV module. The obtained temperature of the PV cell was around 58.10576 °C, 58.1053 °C, 58.105°C, and 58.10468 °C respectively, at solar radiation, ambient temperature, and wind speed of 1000 W/m<sup>2</sup>, 30 °C, and 1 m/s, respectively. It is found that the results are very slightly affected by the mesh size in the investigated range. This is because the computational domain consists of multiple solid domains without a fluid. As a result, only the energy equation is solved, allowing for convergence criteria of less than 10<sup>-15</sup> in the solution of the energy equation.

### **3. Model validation**

Three sets of validation steps were conducted. First, the validation of the solar radiation estimation model is carried out for horizontal and different oriented surfaces. Second, the thermal modeling of a mono-facial PV cell is compared with the data in the literature. Lastly, the thermal model developed for the bi-facial PV module was validated with recent data available in the literature based on the predicted temperature.

#### **3.1 Solar radiation model validation**

In this part, the estimated solar radiation model on a horizontal surface was compared with the measured data published by the National Renewable Energy Laboratory (NREL) at the same location in Sharjah, UAE. It was noticed that the in-house code reasonably estimates the radiation on a horizontal surface, as depicted in Figure 2a. Furthermore, the same code was employed to evaluate the solar radiation on different surfaces tilted at 90° and oriented in various orientations. These data were obtained by changing the surface azimuth angle. The data predicted by the code were compared with the data available in [44]. A reasonable agreement was found, as shown in Figure 2b. The difference may be attributed to the approximations existing in the utilized ASHRAE solar radiation model.

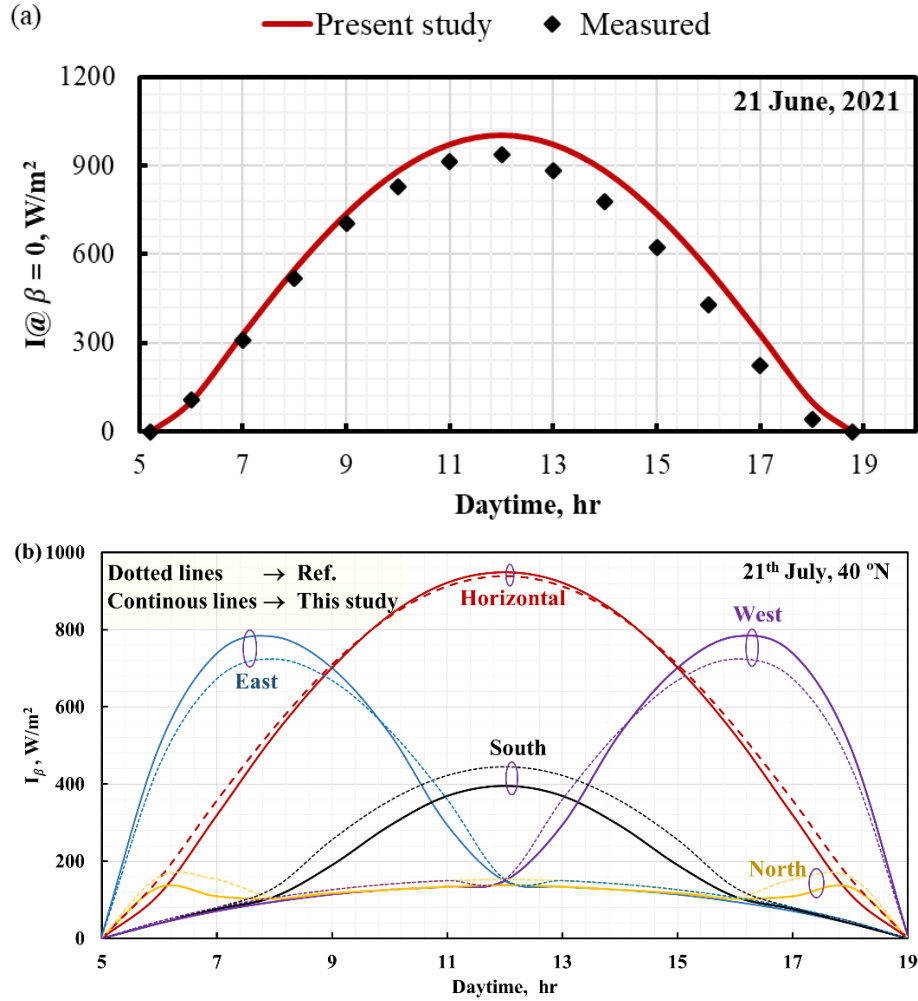


Figure 2: Validation of the solar radiation model with the measured data in Sharjah, UAE (a) given by NREL and (b) with the data available in [44].

### 3.2 Bi-facial photovoltaic cell model validation

In this validation step, the predicted temperatures of the bi-facial PV cell were compared with various mathematical models available in the literature, as listed in Table 3. These models predicted the PV cell temperature as a function of the meteorological conditions, including the wind speed, the ambient temperature, and the received solar radiation from both the rear and front faces. At certain weather conditions, the x-axis in Figure 3 represents the data predicted from the current model, while the y-axis represents the estimated values using the models in Table 3. It can

be observed that the predicted PV cell temperatures are in good agreement with the data obtained from the models in the literature; they are specifically closer to data generated from models (1) and (4). Based on the data given in Figure 3, it can be concluded that the predicted cell temperature is very close to models (1) and (4) with average errors of 2.1% and 2.4%, respectively, while the obtained numerical results are far from models (8) and (7) with average deviations of around 6% and 8%, respectively.

There are several models used for estimating PV cell temperatures. Some use electrical parameters, and others use weather conditions, including the ambient temperature, wind speed, reference electrical efficiency, and the received solar radiation, to evaluate the operating cell temperature. This validation step used these models to conduct the validation as detailed in used in Table 3 [39, 45].

Table 3: Different mathematical models used to evaluate the operating temperature of the PV cell.

Models	Model governing equation
Model (1), [46]	$T_{bi} = T_{amb} + \frac{\alpha_{front}I_{front} + \alpha_{rear}I_{rear}}{U}$ <p>Where <math>\alpha</math> is the absorption coefficient for both front and rear sides and <math>U</math> is total heat transfer coefficient of the PV module. This value was around 29 to 31 W/m<sup>2</sup>.°C in [45]. In this study, the estimated values from the CFD simulation was around 28 up to 39 W/m<sup>2</sup>.°C depending on the weather conditions.</p>
Model (2), [47]	$T_{bi} = T_{amb} + \frac{(I_{front} + I_{rear}) \times (NOCT - 20)}{800}$ <p>The NOCT was taken equal to 47°C as mentioned in [47].</p>
Model (3), [45]	$T_c^t = T_{amb} + \frac{(I_{total})}{800} \times (NOCT - 20) \times (1 - \eta_m) \times \left( \frac{9.5}{5.7 + 3.8 \times v_w} \right)$
Model (4), [45]	$T_c^s = T_{amb} + 0.0138(I_{total}) \times (1 + 0.031T_{amb}) \times (1 - 0.042v_w) \times (1 - 1.053\eta_m)$ <p>Where the temperatures, wind speed, and solar radiations are in °C, m/s, and W/m<sup>2</sup> respectively.</p>
Model (5), [45]	$T_c^c = 0.943T_{amb} + 0.028(I_{total}) - 1.528 \times v_w + 4.3$

Model (6), [45]	$T_c^l = 30.006 + 1.14(T_{amb} - 25) + 0.0175(I_{total} - 300)$
Model (7), [45]	$T_c^k = T_{amb} + 0.0175(I_{total})e^{-3.473-0.0594v_w}$
Model (8), [45]	$T_{bi} = -0.00491T_c^t + 2.05398T_c^s - 0.77271T_c^c - 2.01659T_c^l + 1.01839T_c^k$
Model (9), [48]	$T_c = 0.943 \times T_{sc} + 0.028 \times I_{POA} - 1.528v_w + 4.3$
Model (10), [48]	$T_c = T_a + 0.022I_{total}(1 + 0.009T_{amb})(1 - 0.063v_w)$
Model (11), [47]	$T_c = T_a + \left(\frac{9.5}{5.7 + 3.8v_w}\right) \left(\frac{G}{800}\right) (NOCT - 20)$

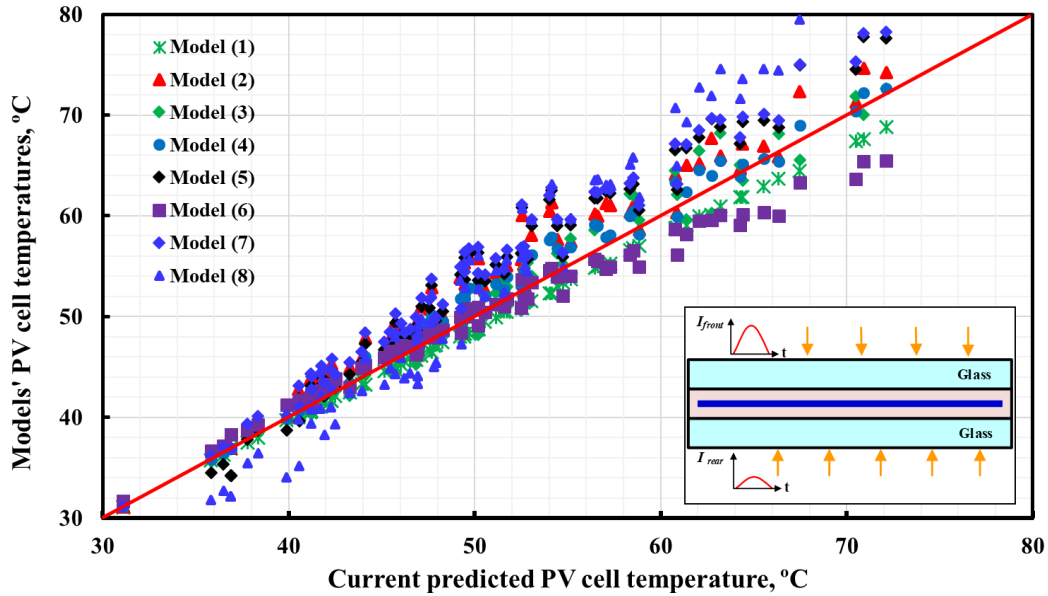


Figure 3: Comparison of the predicted temperature of the bi-facial PV cell with different models available in the literature.

### 3.3 Mono-facial photovoltaic cell model validation

A further validation step was conducted to validate the thermal model of the mono-facial PV cell via two steps. The first step compared the predicted solar cell temperature with the computational result developed by Zhou *et al.* [40]. The same geometry and boundary conditions used in [40] were applied in the current computational model, and the results showed good agreement between them (see Figure 4a). Furthermore, the empirical models in Table 3 were compared with the results obtained from the computational model of this study, as depicted in Figure 4b. A good agreement

was also observed. The computational results are well fitted with the data obtained from models (9), (10), and (11), with average deviations of around 2.6%, 6.2%, and 5.7%, respectively.

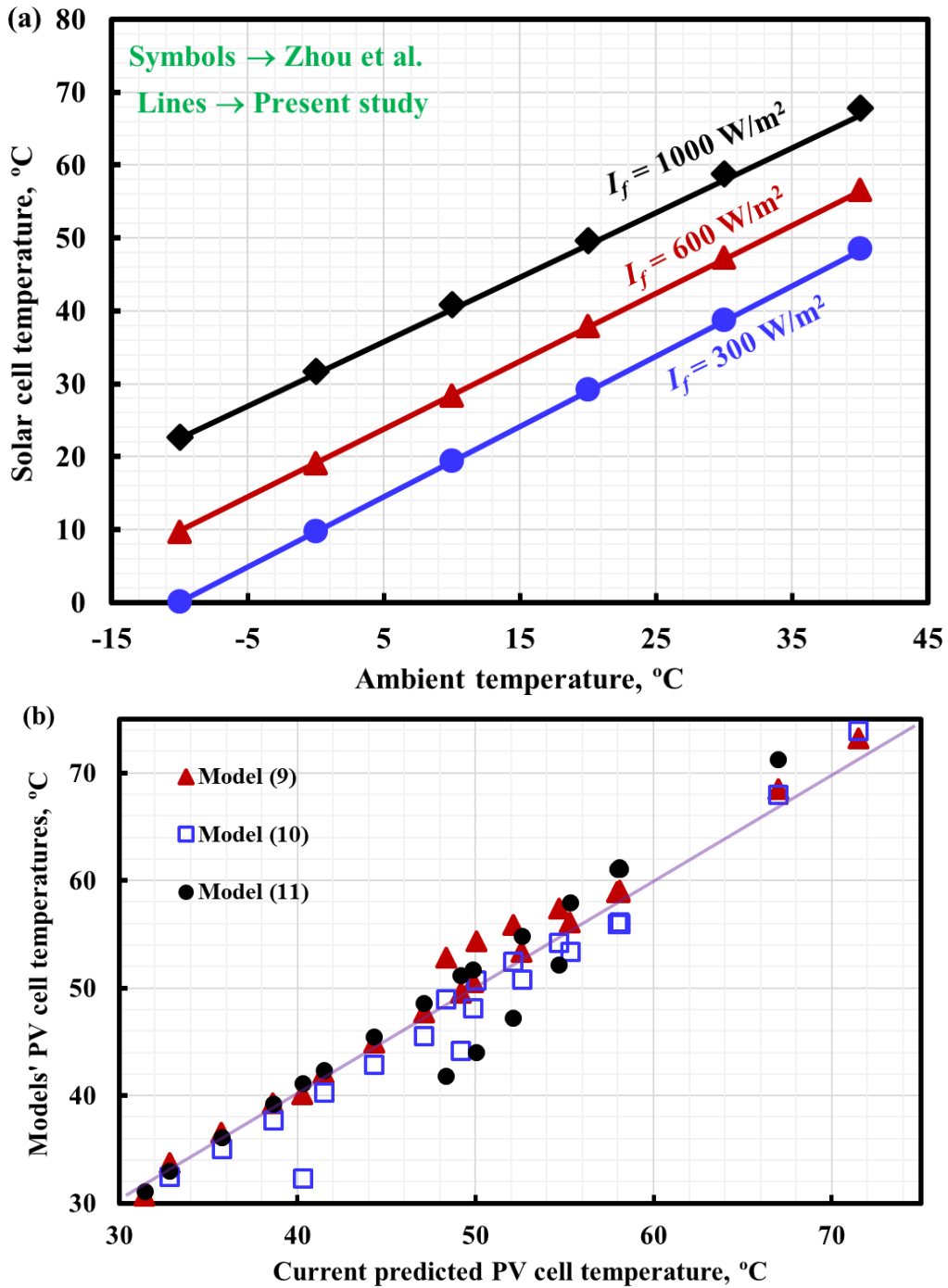


Figure 4: Comparison of the predicted temperature of the mono-facial PV cell with (a) Zhao *et al.* [40], and (b) different empirical models obtained from the literature.



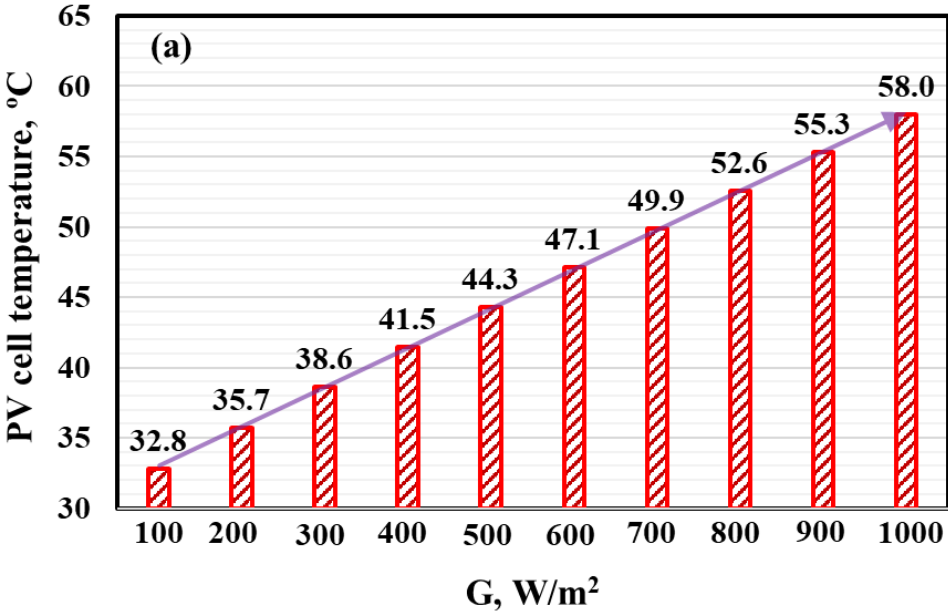
## 4. Results and discussion

In the current work, six main factors that affect the performance of a PV cell were investigated: solar radiation, ambient temperature, wind speed, albedo, rear side absorptivity, and orientation. The influence of these factors on the PV cell temperature, PV cell efficiency, output power, and total energy generated was studied for both mono-facial and bi-facial PV cells. In this study, PV cells covered 90% of the bi-facial PV's back side.

### 4.1 Effect of weather condition parameters on the performance of the mono-facial PV

In this section, the back side absorptivity was not taken into consideration, similar to previous studies that investigated mono-facial PV, in order to examine the influence of other factors. The effect of received solar radiation on the PV cell temperature and efficiency is presented in Figure 5. As shown in Figure 5a, as the solar radiation increases, the PV cell temperature increases too, which causes the efficiency to drop (see Figure 5b). While maintaining all other conditions constant, the result reveals the relation between the PV cell temperature and efficiency. When the solar radiation increases from 100 to 1000 W/m<sup>2</sup>, the PV cell temperature increases from 32.8°C to 58.0°C, while the efficiency decreases from 14.5% to 12.8%. For every 100 W/m<sup>2</sup> change in the solar radiation, the PV cell temperature changes by approximately 2.8°C and its efficiency by 0.189%. Both the temperature and efficiency varied linearly with the change in solar radiation. However, this result does not agree with that of Basher *et al.* [49], where there was no continuous proportional relation. In their study, there were two different efficiency jumps when the solar radiation was less than 200 W/m<sup>2</sup>, while it started to decrease gradually after exceeding this value. They confirmed that this drop resulted from the increase in PV cell temperature, similar to the current study.

On the other hand, the drop in efficiency does not indicate a decrease in the generated power, which can be observed in the study carried out by Karafil [50]. In [50], two simulation programs (MATLAB and PSIM) were used to confirm that the generated power increases as the solar radiation increases. This relation was confirmed under all investigated ambient temperatures (0°C, 25°C, and 50°C).



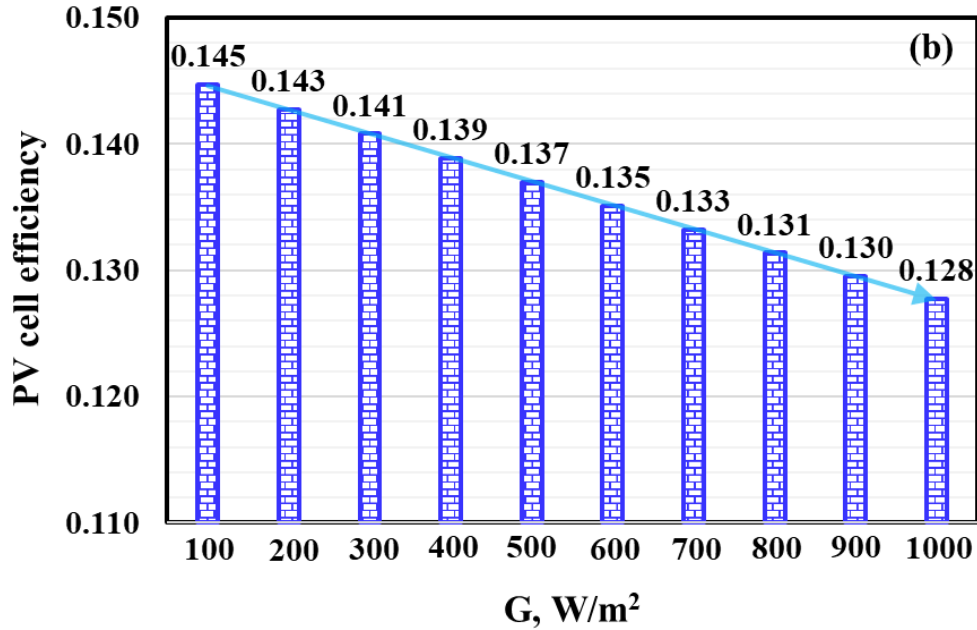


Figure 5: Variation of the (a) estimated PV cell temperature, and (b) estimated PV cell electrical efficiency with the solar radiation at a wind speed of 1 m/s and ambient temperature of 30 °C.

In contrast to the effect of solar radiation, the wind speed shows a positive impact on the PV cell efficiency (see Figure 6b). This is due to the decrease in PV cell temperature, which results from the improvement in air-cooling performance as the wind speed increases (see Figure 6b). For example, when the wind speed increases from 1 to 5 m/s, the PV cell temperature decreases from 58.0°C to 48.3°C, while the efficiency rises from 12.8% to 13.5%. This shows that the temperature and efficiency have a change rate of 2.4°C and 0.15% per 1 m/s, respectively. This confirms the significant relation between the PV cell temperature and efficiency since as the temperature changes by 1°C, the efficiency changes by 0.062%, referring to Figure 6, which is almost similar to that presented in Figure 5 with a change of 0.067%.

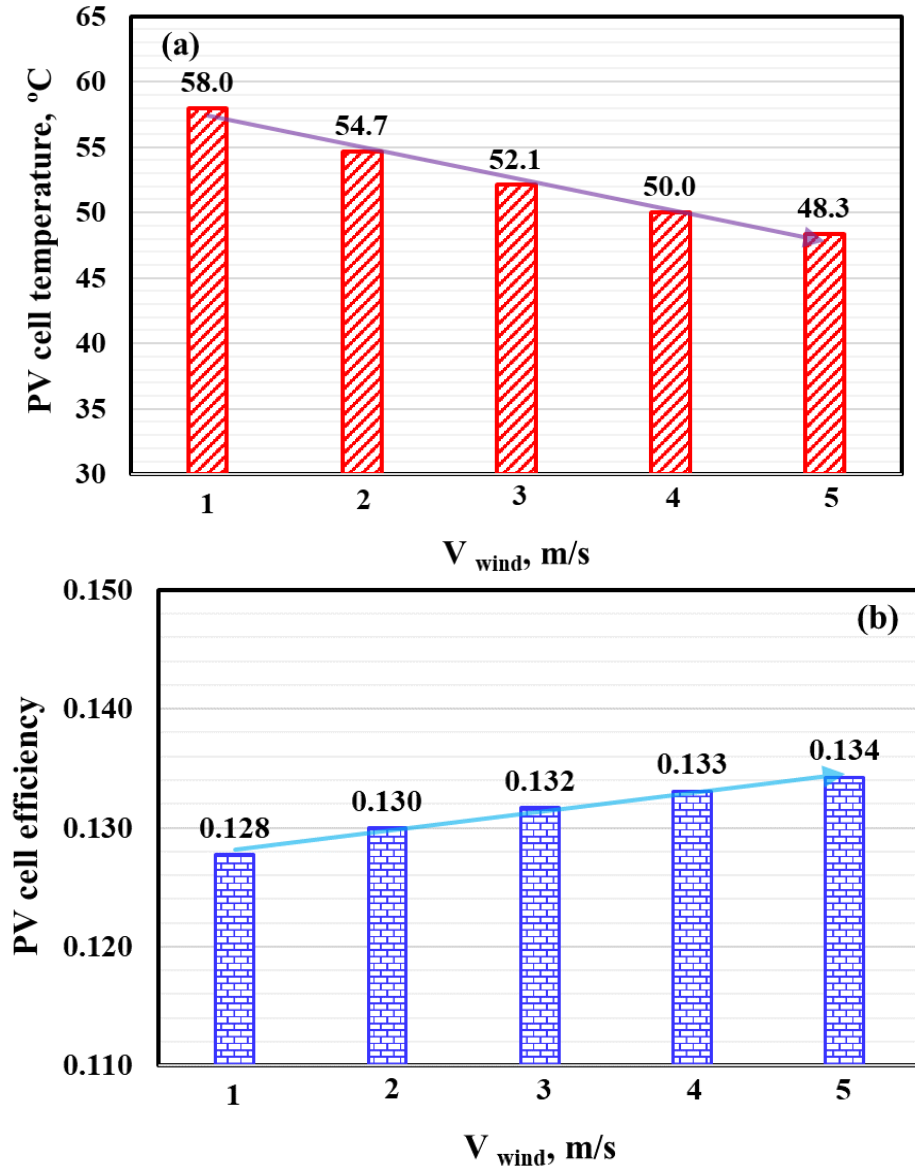
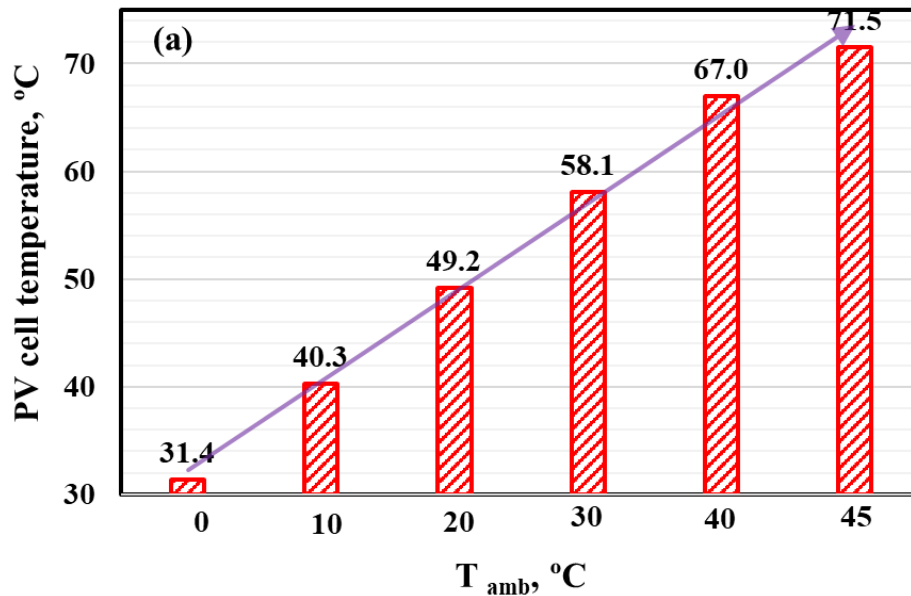


Figure 6: Variation of the (a) estimated PV cell temperature, and (b) estimated PV cell electrical efficiency with the wind speed at solar radiation of  $1000\text{W}/\text{m}^2$  and ambient temperature of  $30^\circ\text{C}$ .

The effect of ambient temperature is similar to that of solar radiation such that it is directly proportional to the PV cell temperature and inversely proportional to the efficiency (see Figure 7).

However, the rate of change is higher in this case, where the PV cell temperature increases from  $31.4^\circ\text{C}$  to  $71.5^\circ\text{C}$  and the efficiency decreases from 14.6% to 11.9% as the ambient temperature increases from  $0^\circ$  to  $45^\circ\text{C}$ . These correspond to change rates of  $0.89^\circ\text{C}$  and 0.06%, respectively,

while the relation between the PV cell temperature and efficiency is still the same as those presented in Figure 5 and Figure 6 (~0.065% per 1°C). The reason behind the high effect of ambient temperature on the PV cell temperature compared to that of solar radiation is that the former affects the power generated by the cell negatively. As an example, in [50], the maximum power generated decreased from 112.2 to 89.66 W when the ambient temperature increased from 0°C to 50°C at a solar radiation of 1000 W/m<sup>2</sup> based on the MATLAB simulation results. This necessitates the use of cooling mechanisms at high ambient temperatures to decrease the PV cell temperature and hence improve its efficiency [51-56].



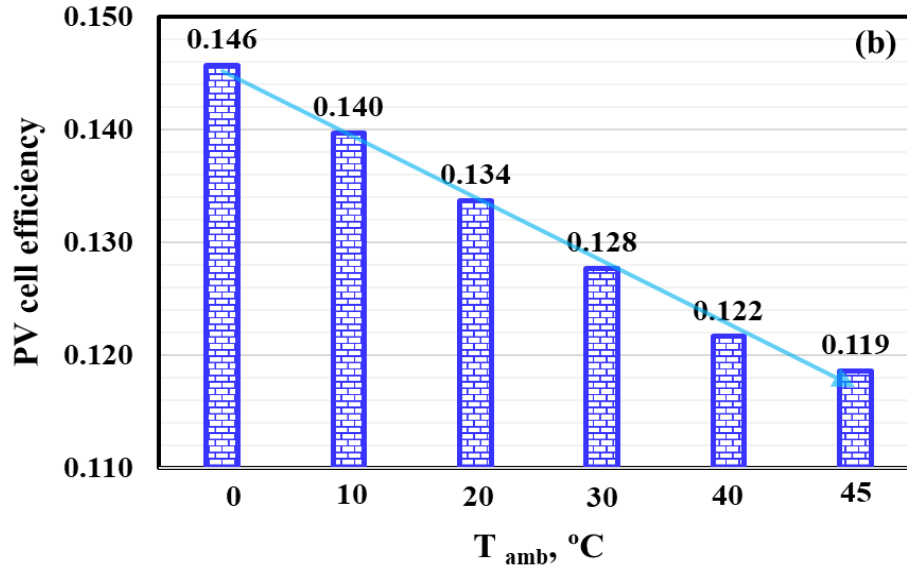


Figure 7: Variation of the (a) estimated PV cell temperature, and (b) estimated PV cell electrical efficiency with the ambient temperature at solar radiation of 1000W/m<sup>2</sup> and wind speed of 1 m/s.

The temperature contours depicted in Figure 8 show the effect of solar radiation and ambient temperature on the top glazing temperature of the mono-facial PV cell. All contours display the same pattern but with different scales. As an example, when the solar radiation is 1000 W/m<sup>2</sup> and the ambient temperature is 20°C, the temperature at the center is 48.09°C, which then decreases gradually to 47.68°C reaching the corners, which are the farthest points from the center. At the same solar radiation of 1000 W/m<sup>2</sup>, the scale rises by 8.89°C when the ambient temperature increases from 20°C to 30°C. However, a slight difference is observed at 800 W/m<sup>2</sup>, where the scale rises by 9.09°C considering the same change in ambient temperature. This shows that the influence of these investigated factors is slightly affected by each other as they have a direct impact on the PV cell temperature and efficiency, as presented above in Figure 5, Figure 6, and Figure 7.

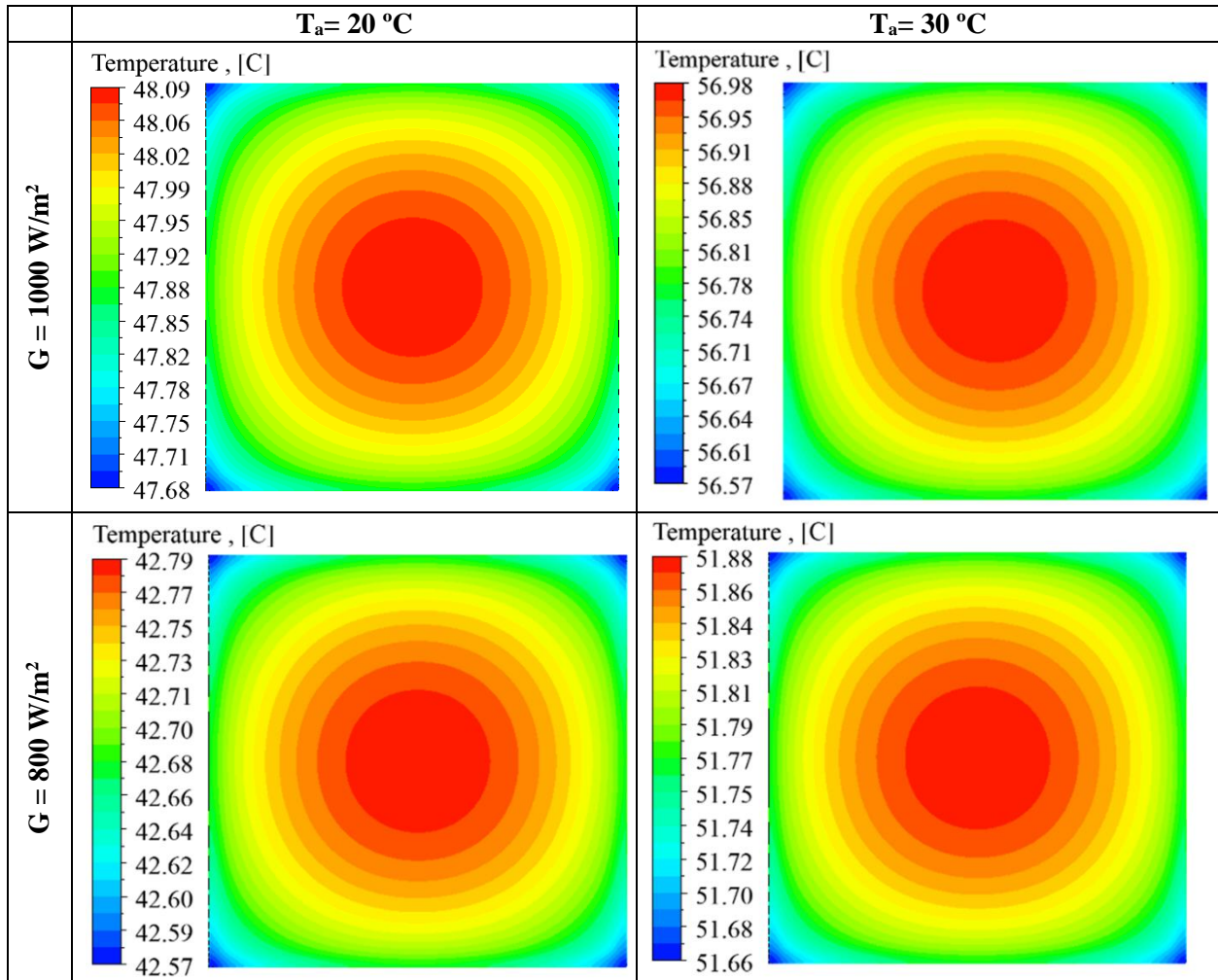
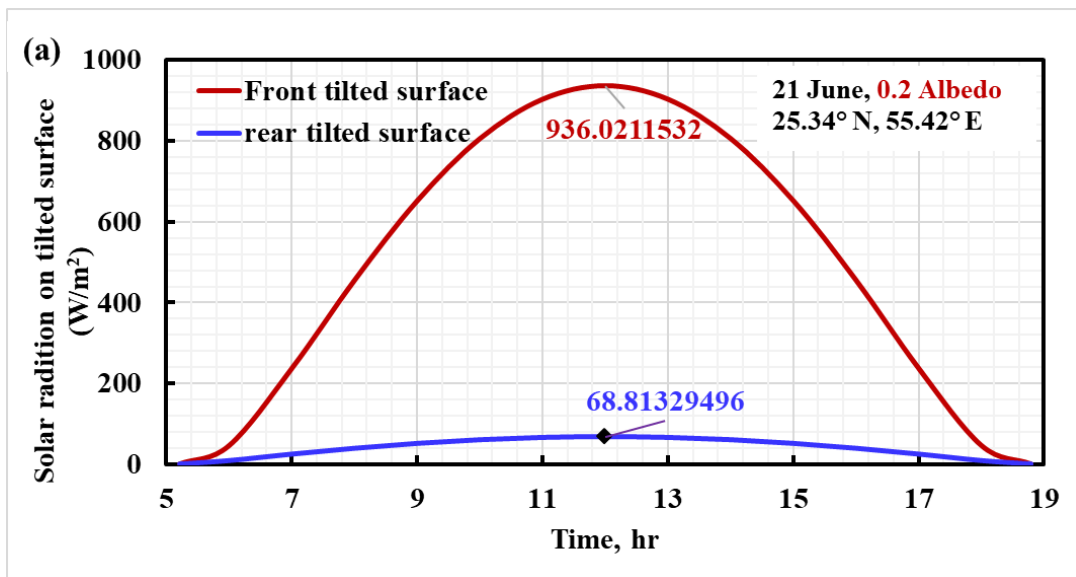


Figure 8: Temperature contours on the top glazing of the mono-facial photovoltaic cell at different conditions.

Figure 9 shows the effect of albedo on the solar radiation received by the front and rear surfaces with an optimal tilt angle. For the three studied albedo values (0.2, 0.5, and 0.7), the received solar radiation peak is at noon for both the front and back sides. The highest received solar radiation by the front surface is not significantly affected by the change in albedo, such that it is 936.02, 950.47, and 960.11  $\text{W/m}^2$  for albedo values of 0.2, 0.5, and 0.7, respectively. On the other hand, as the albedo increases, the maximum received solar radiation by the back side increases significantly. When the albedo changes from 0.2 to 0.7, the solar radiation on the rear surface increases from

60.81 to 226.61 W/m<sup>2</sup>. In other words, the solar radiation received by the rear side at an albedo of 0.5 and 0.7 is higher than that at 0.2 by 2.4 and 3.7 times, respectively. This shows the importance of considering the effects of albedo and nearby surface's reflectivity, as they may remarkably affect the PV performance. The increase in solar radiation received by the rear side of a mono-facial PV may lead to an increase in the PV cell temperature and hence decrease its efficiency. Even though the PV cell is totally insulated from the back side, this solar radiation could be utilized by using the bi-facial configuration rather than being lost, especially at high albedo values, as shown in Figure 9b and Figure 9c. As an example, the amount of solar radiation received by the rear surface (226.61 W/m<sup>2</sup>) is approximately 19% of the solar radiation received by the whole PV (1186.72 W/m<sup>2</sup>).





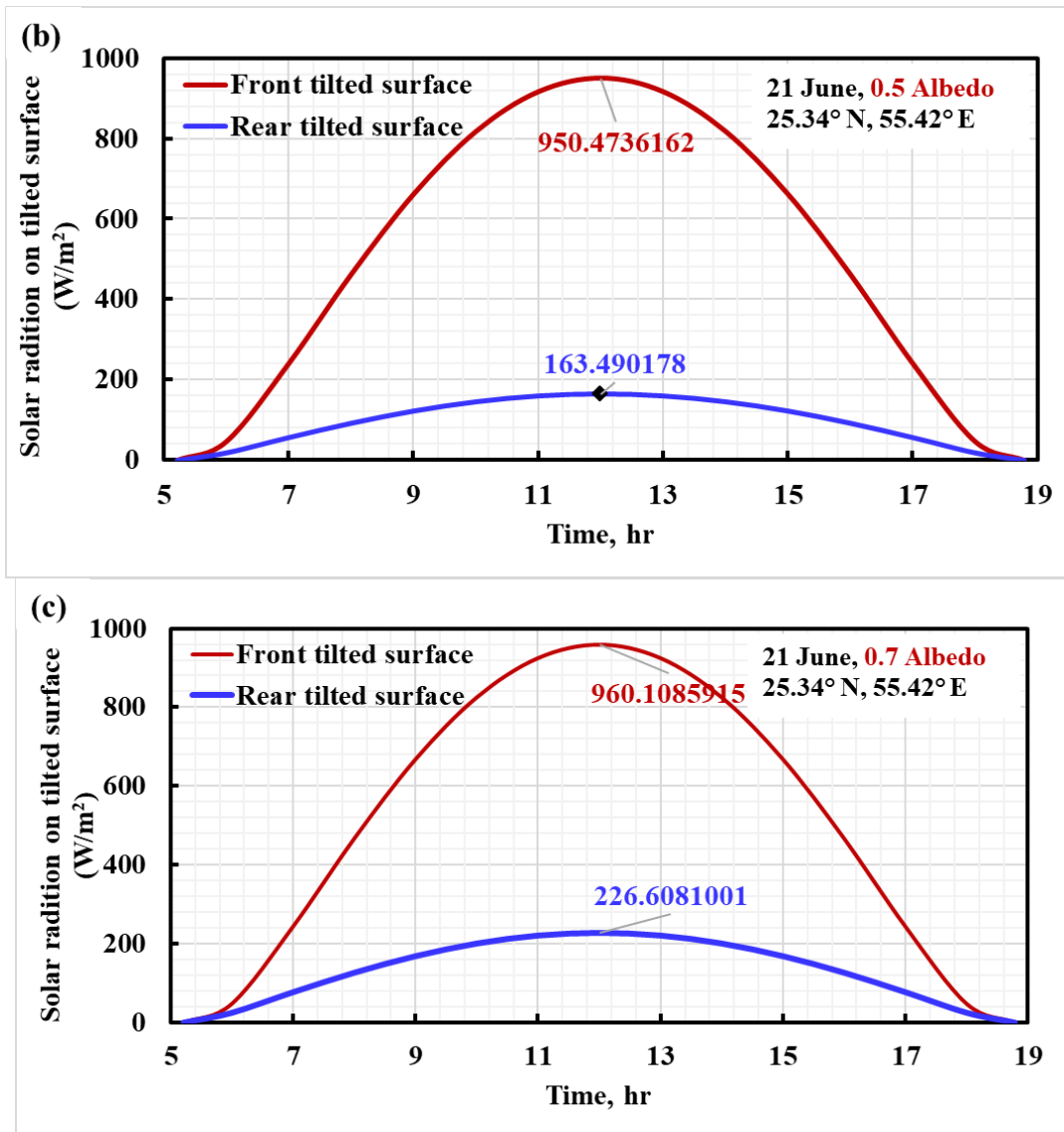
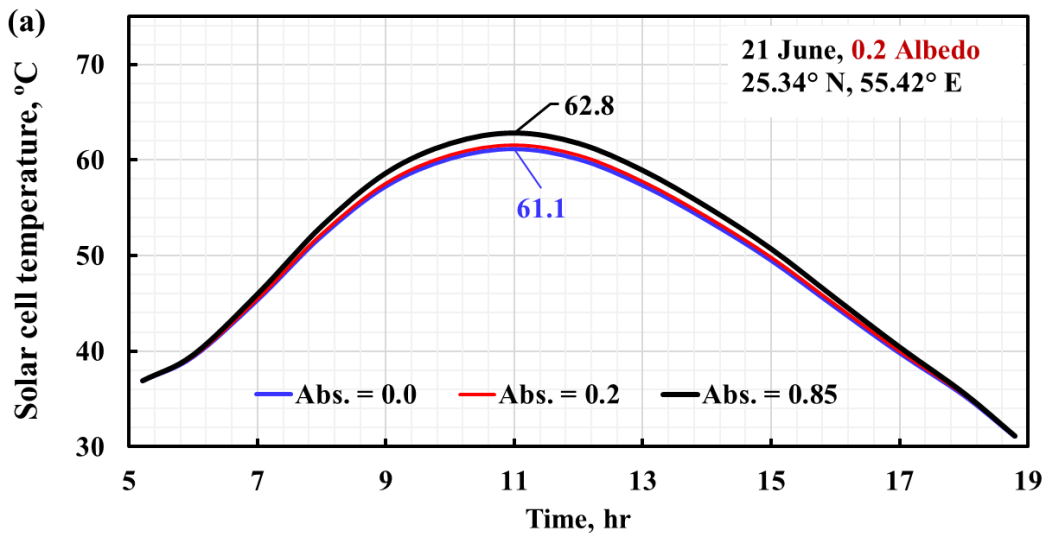


Figure 9: Variation of the front and rear estimated solar radiation on a surface tilted with optimal year-long tilt angle at (a) albedo = 0.2, (b) albedo = 0.5, and (c) albedo = 0.7 for the location of Sharjah (25.34° N, 55.42° E).

#### 4.2 Effect of TPT layer rear side absorptivity on the mono-facial PV cell

As shown in Figure 9, the solar radiation received by the rear surface of an optimally tilted PV cell could be relatively considerable at high values of albedo. Thus, it is essential to study the effect of this radiation on the thermal performance of a mono-facial PV cell while examining the impact of back side absorptivity, as shown in Figure 10. Previous studies that have investigated mono-facial

PV cells do not consider the effect of back side absorptivity, while in real life it is approximately equal to 0.2. The results in Figure 10 show that the effect of absorptivity is not significant, especially at small values of albedo (see Figure 10a). This could be predicted as the solar radiation reflected on the back side is relatively low at albedo = 0.2, as presented in Figure 9a. However, when the albedo increases from 0.2 to 0.7, the difference between the peak solar cell temperature at absorptivity 0 and 0.2 increases from 0.4°C to 1.4°C. Additionally, this difference corresponds to a specific date and location, which may change considerably if the solar radiation changes. Therefore, considering the effect of the rear surface absorptivity of a mono-facial PV cell contributes to enhancing the predicted results' accuracy. In order to further show the importance of back side thermal resistance, a huge difference between the curves corresponding to absorptivity of 0.2 and 0.85 can be observed. However, 0.85 does not represent an actual example of the TPT layer absorptivity value of PV cells, but improper designs would lead to an increase in the absorptivity reaching values above 0.2.



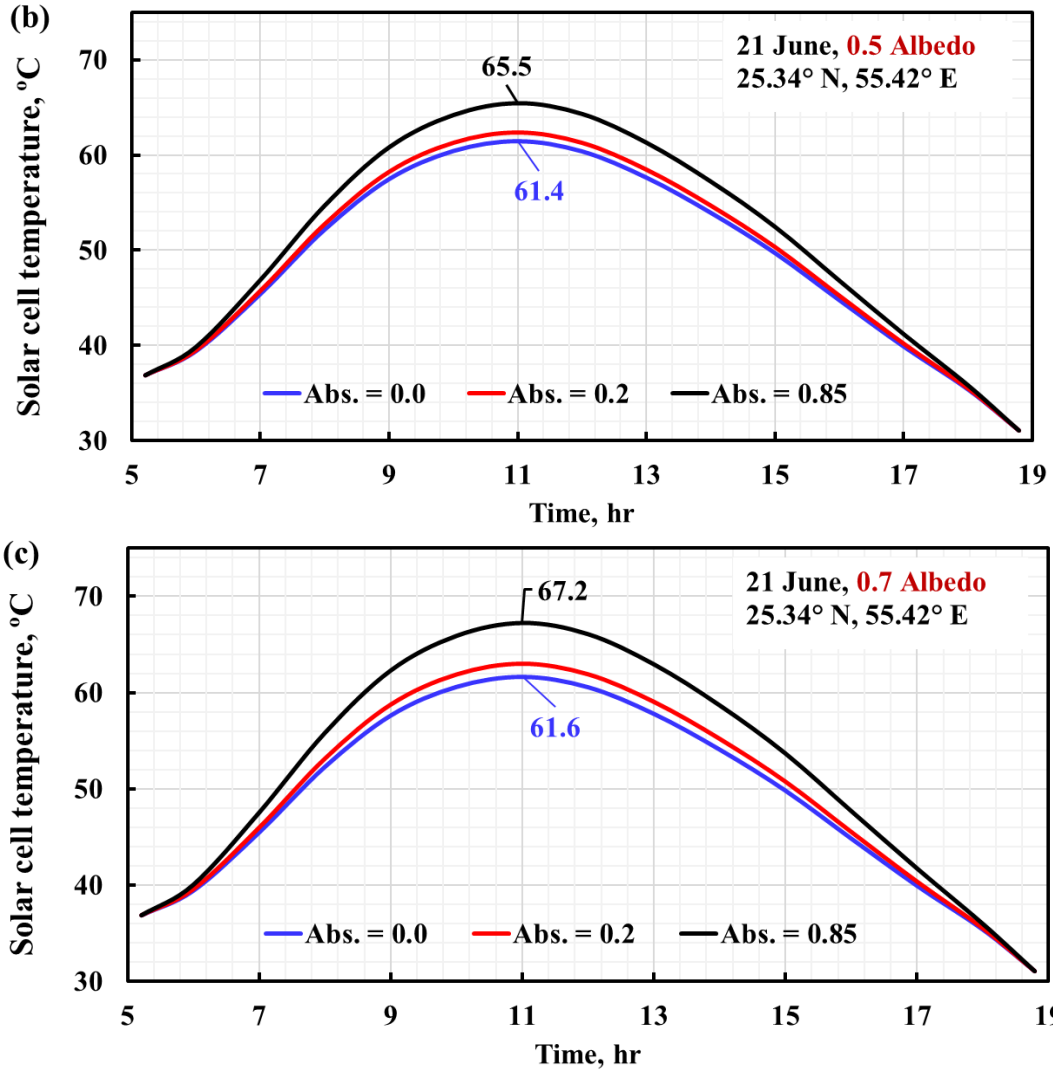
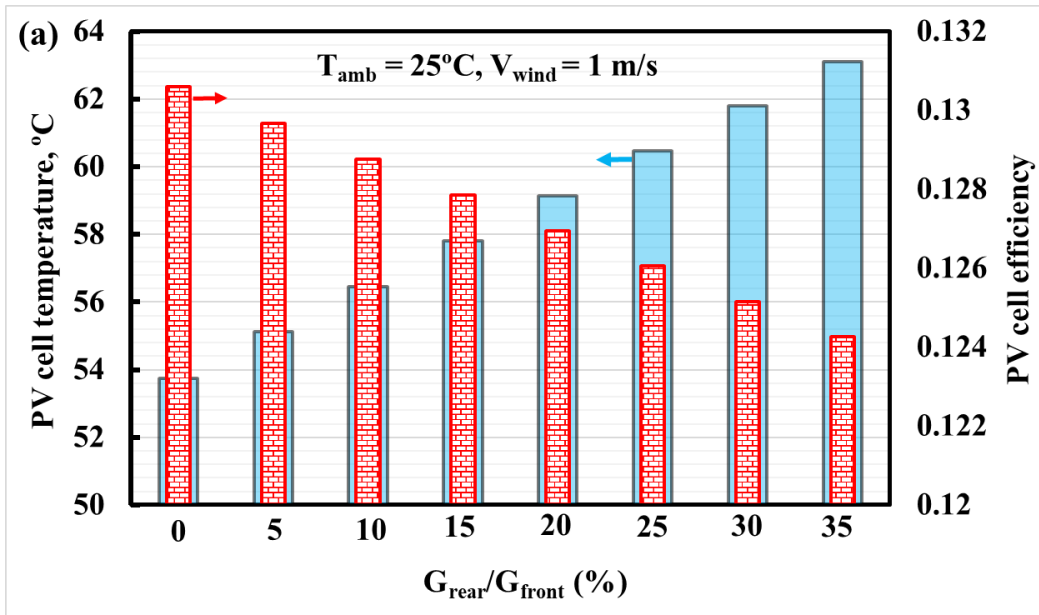


Figure 10: Effect of rear side absorptivity on the optimally tilted mono-facial solar cell temperature at (a) albedo = 0.2 and (b) albedo = 0.5, and (c) albedo = 0.7.

### 4.3 Performance of bi-facial PV cell

The effects of rear-to-front solar radiation, ambient temperature, and wind speed on the performance of a bi-facial PV cell are presented in Figure 11. The rear-to-front solar radiation and ambient temperature show a negative effect, while the wind speed shows a positive effect on the PV cell efficiency [57]. The relation between PV cell temperature and efficiency is the same as that obtained for the mono-facial PV cell, with an efficiency change rate of 0.067% per 1°C.

Additionally, the effect of ambient temperature and wind speed on the bi-facial PV cell performance is similar to that on the mono-facial PV cell, as shown in Figure 6 and Figure 7. However, higher PV cell temperatures and lower efficiency are noticed in the case of bi-facial PV. This is due to the difference between the TPT layer and glass absorptivity that are placed on the back sides of mono-facial and bi-facial configurations, respectively. Another difference between the performance responses of the two configurations is the sensitivity to the investigated variables. As an example, when the wind speed changed by 1 m/s, the PV cell temperature and efficiency changed by 2.4°C and 0.15% for mono-facial PV, while in the case of bi-facial PV, they changed by 4.05°C and 0.27%, respectively. On the other hand, the sensitivity to the ambient temperature of mono-facial and bi-facial PV cells is almost the same such that the change rate of PV cell temperature is 0.86-0.89°C and that of efficiency is 0.058-0.06% per 1°C of ambient temperature change.



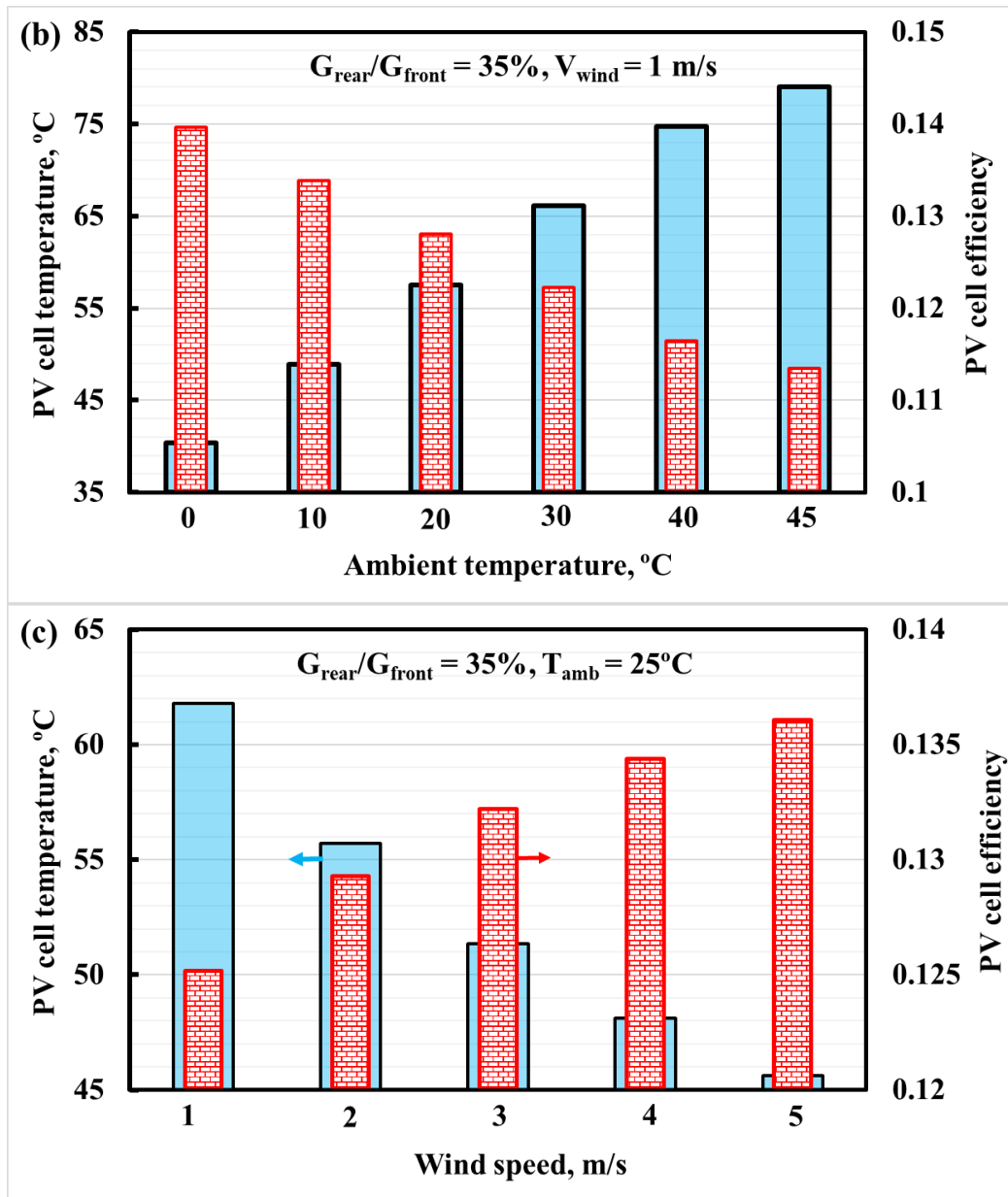
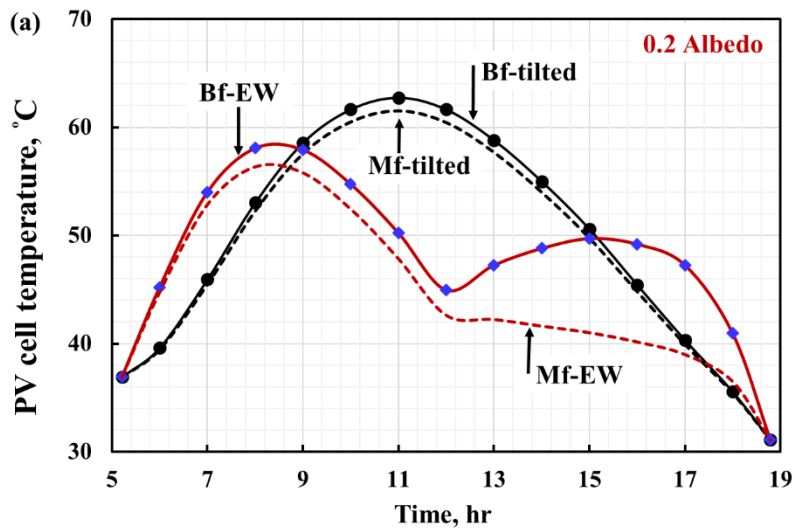


Figure 11: Effect of (a) rear to front solar radiation ratio, (b) ambient temperature, and (c) wind speed on the predicted bi-facial PV cell temperature.

#### 4.4 Comparison of mono-facial and bi-facial PV cells

The absorptivity of the mono-facial PV back-side is taken as 0.2 in this section. A comparison between the mono-facial and bi-facial PV cells temperatures is demonstrated in **Error! Reference source not found.** under different albedo values and orientations. In all cases, the mono-facial and

bi-facial tilted PV cells show similar patterns of temperatures with different peaks. However, the predicted cell temperatures of the mono-facial cell are slightly less than the bi-facial at the same time. This is because the bi-facial cell absorbs two radiation components from the rear side and the frontal side of the PV cell. This difference in the temperature becomes high after the solar noon for the vertical modules. Also, two temperature peaks are observed for the E-W oriented bi-facial module because the solar radiation received by the bi-facial vertical module has two peaks; one at the morning time around 9:00 AM and the other around 3:00 PM. The difference between the highest temperatures of the bi-facial vertical module at these times resulted from the change in the ambient temperature and wind speed.



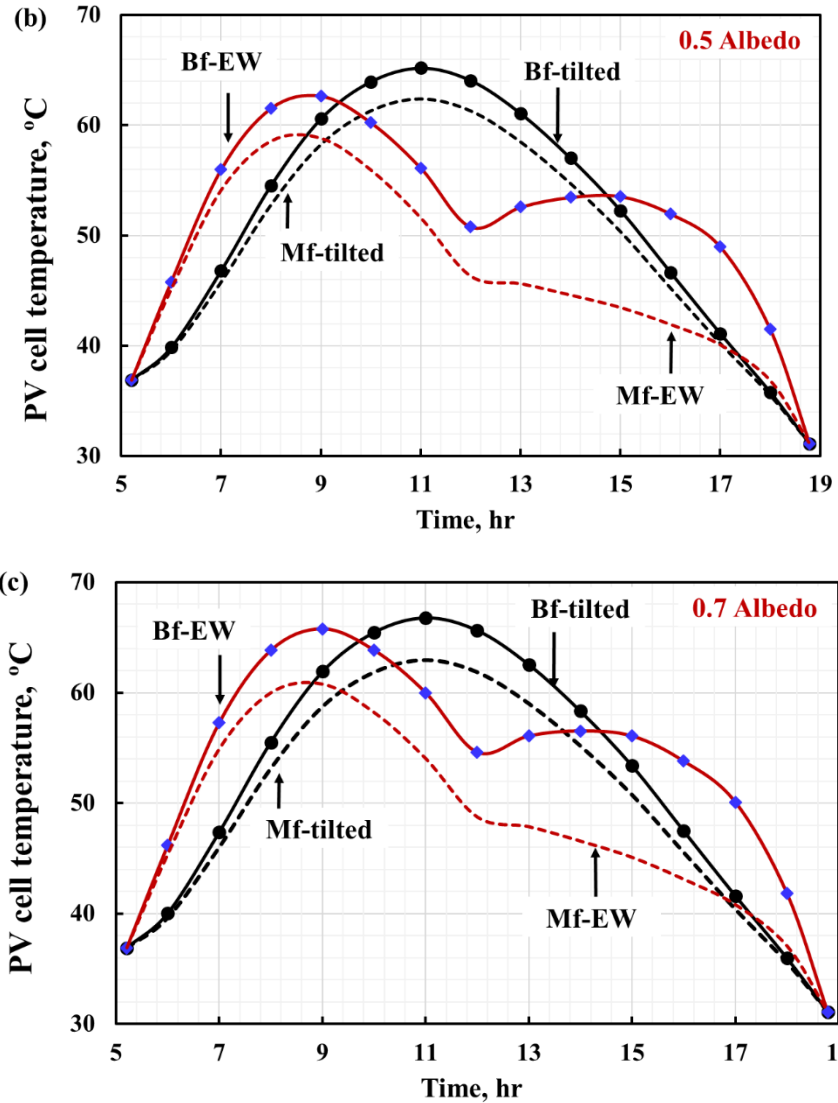


Figure 12: Comparison of the PV modules temperatures of the mono-facial (Mf) and bi-facial (Bf) PV cells per unit area on the 21<sup>st</sup> of June at (a) albedo = 0.2, (b) albedo = 0.5, and (c) albedo = 0.7.

#### 4.5 Year-long comparison

The objective of this section is to compare the annual energy production of four different PV systems. The PVsys simulation tool is used in this section. Four configurations of PV systems are simulated to demonstrate the difference between two different technologies (bi-facial and mono-facial solar panels). The simulation is conducted for a PV system with designed capacity of 5 kW<sub>p</sub>,

which was attained using mono-facial and bi-facial PV modules with the same inverter. The characteristics of the PV modules and the used inverter are detailed in Table 4 and Table 5, respectively.

Table 4: Selected PV module specifications.

Parameter	LG Solar LG400N3K-V6 NeON H+ Black (Bi-facial)	LG Solar LG400Q1C-A6 NeONR (Mono-facial)
Cells	132 Cells	60 Cells
Cell Type	Monocrystalline/N-type	Monocrystalline/N-type
Manufacturer	LG	LG
Maximum Power P <sub>max</sub> (W)	400	400
MPP Voltage V <sub>mpp</sub> (V)	37.2	37.2
MPP Current I <sub>mpp</sub> (A)	10.76	10.76
Open Circuit Voltage (V <sub>oc</sub> , ± 5%) (V)	45.2	43.8
Short Circuit Current (I <sub>sc</sub> , ± 5%) (A)	11.16	11.32
Module Efficiency (%)	20.4	22.1
Power Temperature Coefficient	-0.33 %/°C	-0.29 %/°C
Price	€247 [58]	€238.66 [59]

Table 5: Selected Inverter Specifications [60].

Parameter	SOFAR 5000TLM
<b>Max. input power</b>	5200 W
<b>Max DC power for single MPPT</b>	3000 W (200 V-500 V)
<b>Number of independent MPPT</b>	2
<b>Max input voltage</b>	600V
<b>Rated input voltage</b>	360V
<b>Operating input voltage range</b>	100 V - 550 V
<b>Input short circuit current for each MPPT</b>	18A
<b>Max AC power</b>	5000 VA
<b>Max output current</b>	22 A
<b>Max efficiency</b>	97.6%
	40



<b>Ambient temperature range</b>	-25°C ~ +60°C (above 45 °C)
----------------------------------	-----------------------------

The simulation is conducted under the weather conditions of Sharjah, United Arab Emirates for one complete year. The detailed site specifications are shown in Table 6. The simulation is conducted for a system 1.5 m above the ground with albedo of 0.85, module bi-faciality of 0.80 and the optimal tilted modules are tilted at angles of 25.3°.

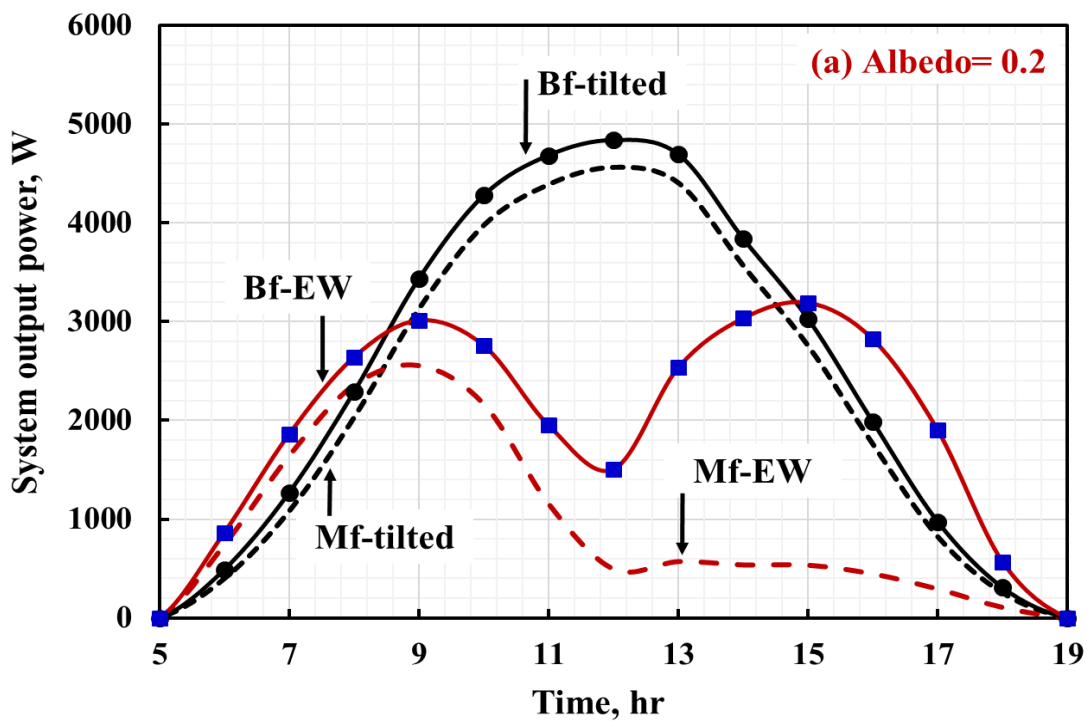
Table 6: Site Specifications.

Location Information	Sharjah, United Arab Emirates
Latitude	25°20'14.53" N
Longitude	55°24'43.42" E
Average DNI	5.80 kWh/m <sup>2</sup> /day
Average DHI	2.02 kWh/m <sup>2</sup> /day
Average GHI	6.03 kWh/m <sup>2</sup> /day
Average temperature	27.7 °C
Average wind Speed	3.7 m/s

Four different scenarios will be compared. First, a 5 kWp bi-facial 90° vertical and east-oriented; second, 5 kWp bi-facial 25.3° tilted and south-oriented; third, a 5 kWp mono-facial 90° tilted and east-oriented; and finally, a 5 kWp mono-facial 25.3° tilted and south-oriented. These will be compared in terms of daily, monthly and yearly energy production.

PV systems were modeled, and samples of the simulated output were collected for the summer solstice. The comparison is depicted in **Error! Reference source not found.** under different albedo values and orientations. In all cases, the mono-facial and bi-facial tilted PV systems show similar patterns with different peaks. The trends presented in **Error! Reference source not found.** agree with the results reported in previous studies [36, 61-64]. The lowest peak corresponds to the

vertical mono-facial PV E-facing for all albedo values. As the albedo increased, the power generated by all PVs increased, and the difference between mono-facial and bi-facial became more considerable, as reported by Gu et al. [65]. The effect of albedo is slightly affecting the optimal tilted mono-facial PV system. However, increasing the albedo increases the peak power generation by the bi-facial modules due to the increase in the received radiation with the increase in the albedo for all systems except the optimal tilted mono-facial system. Further, the albedo also affects the power generated by the mono-facial PV vertical system. It is also noticed that the power generated by the vertical bi-facial PV has two peaks. One at 9:00 AM and the other nearly at 3:00 PM due to the same trend of the received radiation. It is also noticed that the power generated by the bi-facial tilted PV system reached the maximum limit of the inverters, specially when the albedo is high. This results in a flat power generation with respect to time, which is known as the inverter's clipping loss. This phenomenon can be avoided by the appropriate selection of the inverter.



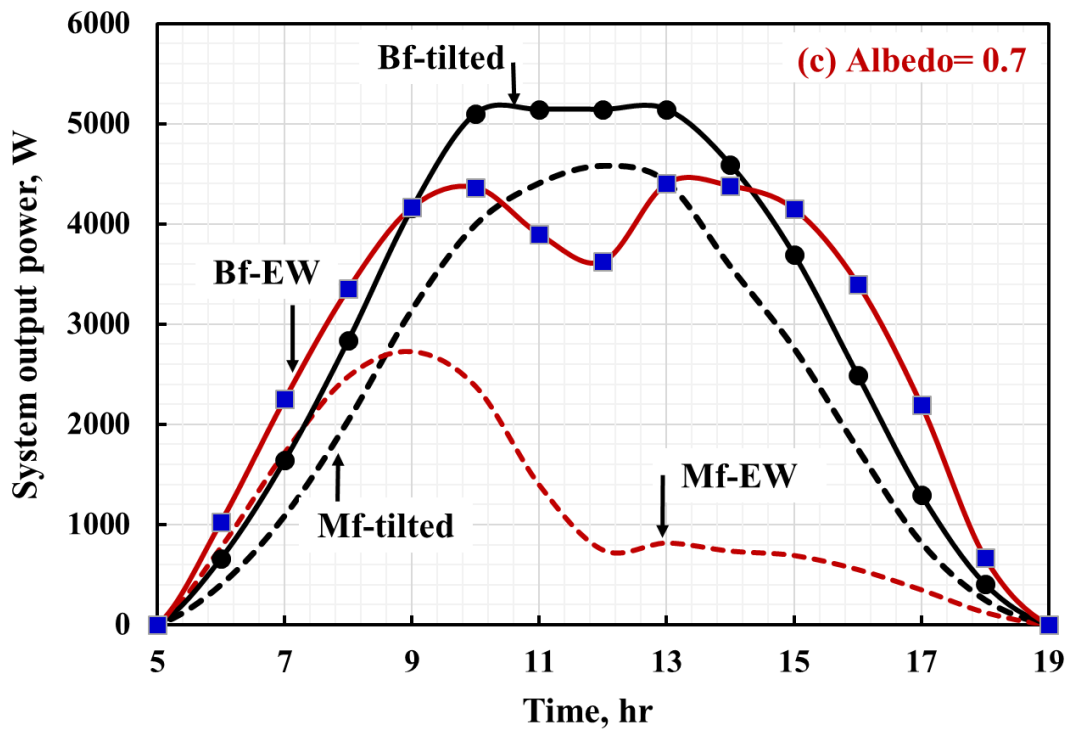
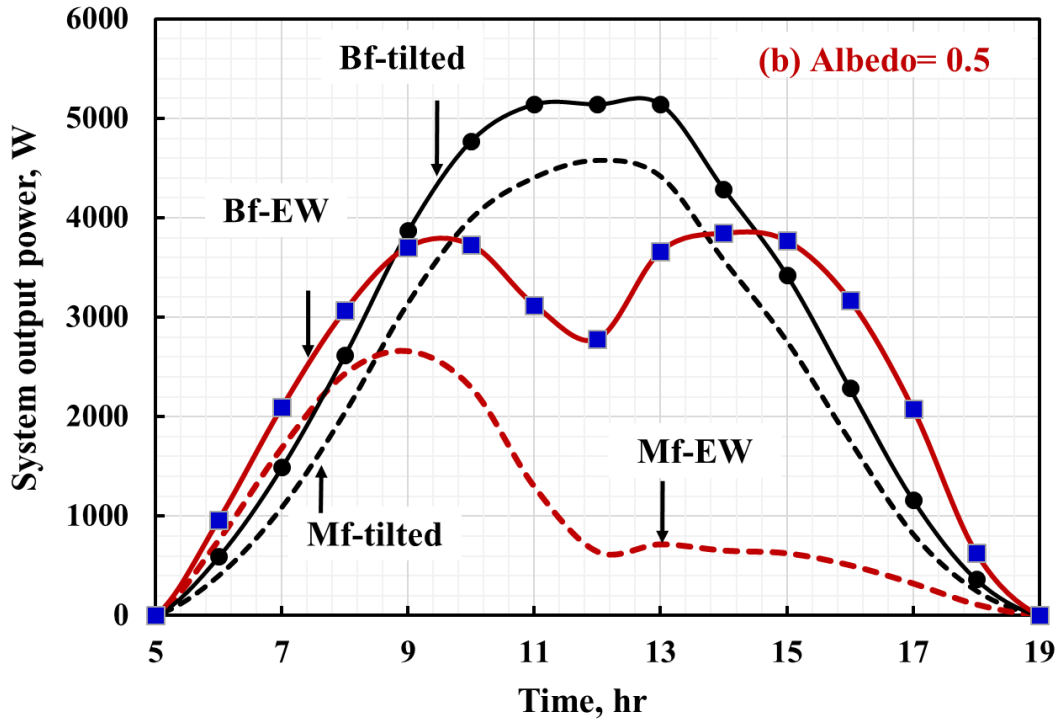


Figure 13: System power generation for 21 June (summer solstice) at (a) albedo= 0.2; (b) albedo= 0.5; and (c) albedo= 0.7 for vertical and tilted mono-facial and bi-facial PV systems.

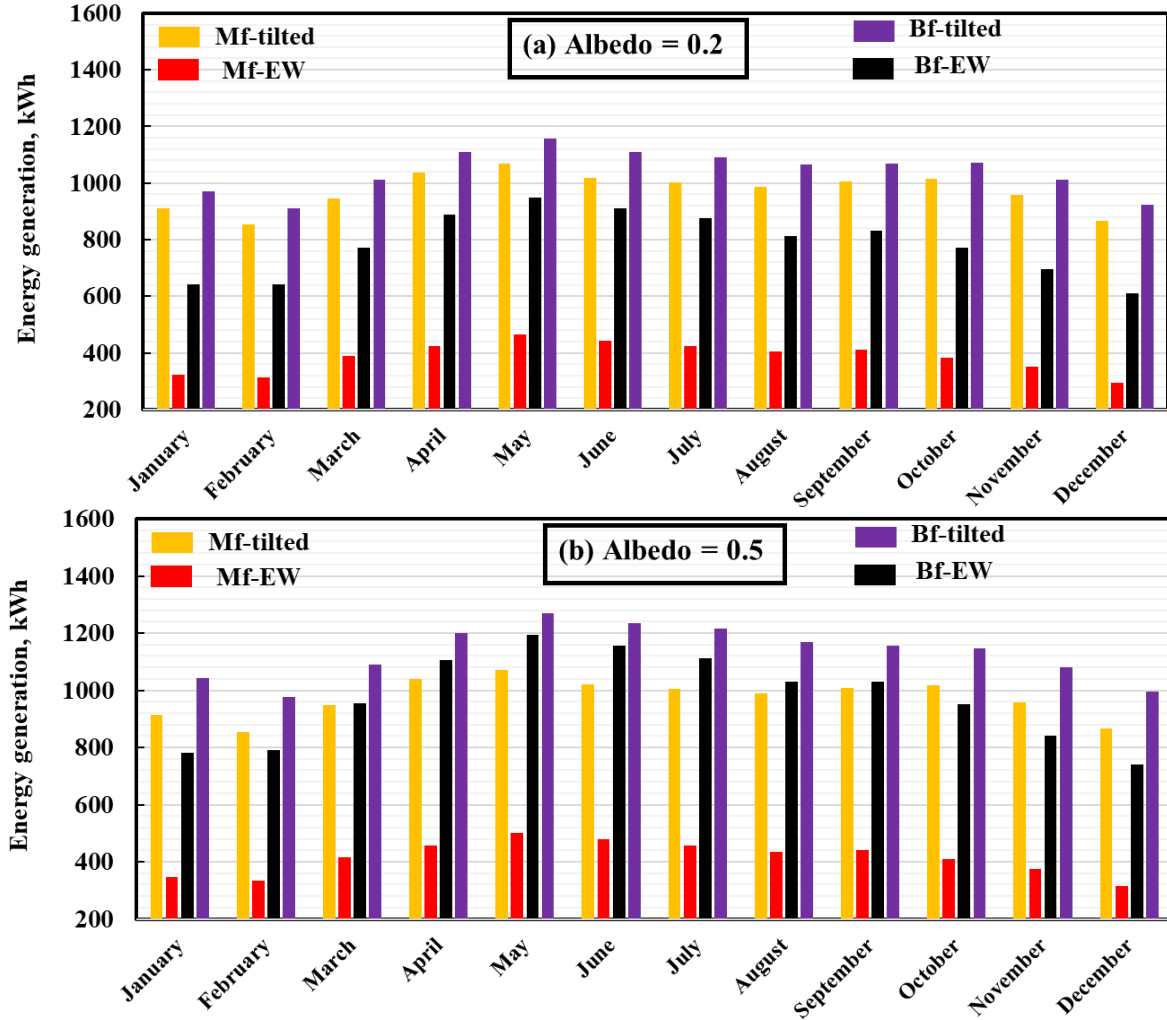
In all cases, as shown in **Error! Reference source not found.**, the effect of albedo on the energy gain was positive through the investigated day [66, 67]. The data in **Error! Reference source not found.** confirms that using the bi-facial PV is favorable under the investigated conditions for Sharjah-UAE. Even at low albedo (e.g., albedo=0.2), the daily electrical energy gain of the bi-facial-tilted (36.11 kWh) was higher than that of the mono-facial-tilted (33.11 kWh) around 9 % increase in the energy gain. As albedo increased from 0.2 to 0.7, the daily electrical energy gain of the bf-tilted increased hugely to 42.3 kWh which represents around 27% increase in the energy gain.

Table 7: Comparison of the output energy for the different installing scenarios of the bi-facial PV compared with the optimal tilted mono-facial PV module at different albedo values.

Albedo	Daily received solar radiation, kWh, (21 June, Sharjah)			
	Tilted, 25°		Vertical mounted	
	Bi-facial	Mono-facial	Bi-facial, vertical E-W	Mono-facial, vertical E-W
0.2	36.11	33.11	28.65	13.57
0.5	40.31	33.21	36.61	14.70
0.7	42.30	33.26	41.86	15.45

The monthly variation of the energy gain from the PV system investigated in this part is depicted in Figure 14 at albedo values of 0.2, 0.5 and 0.7. Generally, it is noticed that increasing the albedo increase the monthly energy generation of the bi-facial PV system and the vertical tilted mono-facial modules. But it is slightly affecting the power generation of the optimal tilted mono-facial PV system. Further, the highest energy generation can be attained by the bi-facial tilted PV module. The energy generation of the bi-facial E-W oriented vertical PV system is less than the conventional mono-facial tilted PV system at low albedo (0.2) and greater at high albedo (0.7). Additionally, in June, the vertical bi-facial PV system attains the highest energy compared to the

other systems at an albedo of 0.7. Further, the vertical oriented mono-facial PV module attained the lowest energy generation in all cases.



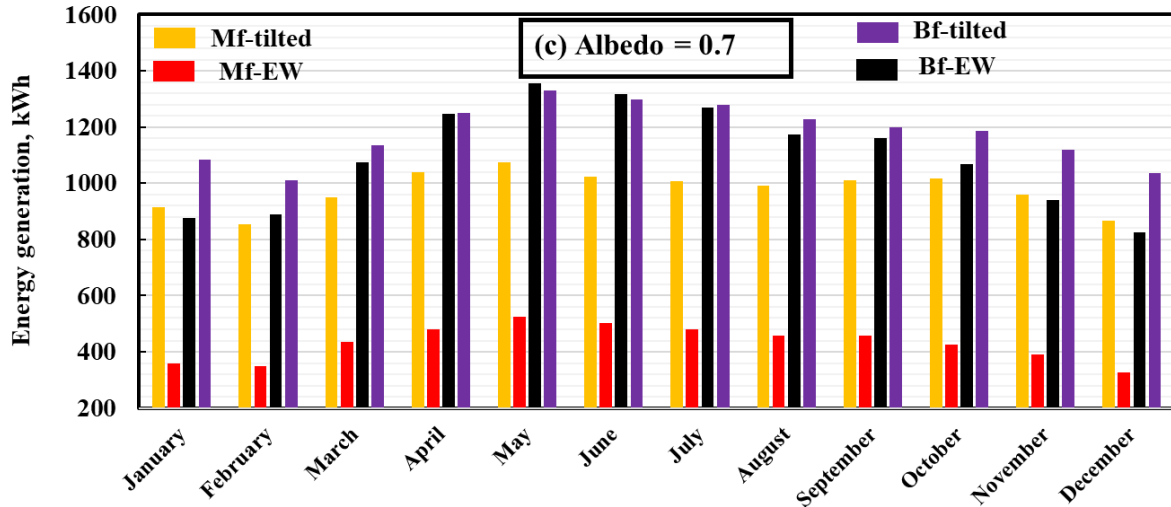


Figure 14: Monthly energy output comparison at (a) albedo= 0.2; (a) albedo= 0.5; (a) albedo= 0.7.

Figure 15 summarizes the annual energy gained by the investigated systems at various albedo values. The tilted bi-facial PV system attained the highest energy followed by the bi-facial vertical then by the mono-facial tilted system at albedo values greater than 0.5. The lowest attained energy gain is for the vertical mono-facial module for the whole investigated albedo values.

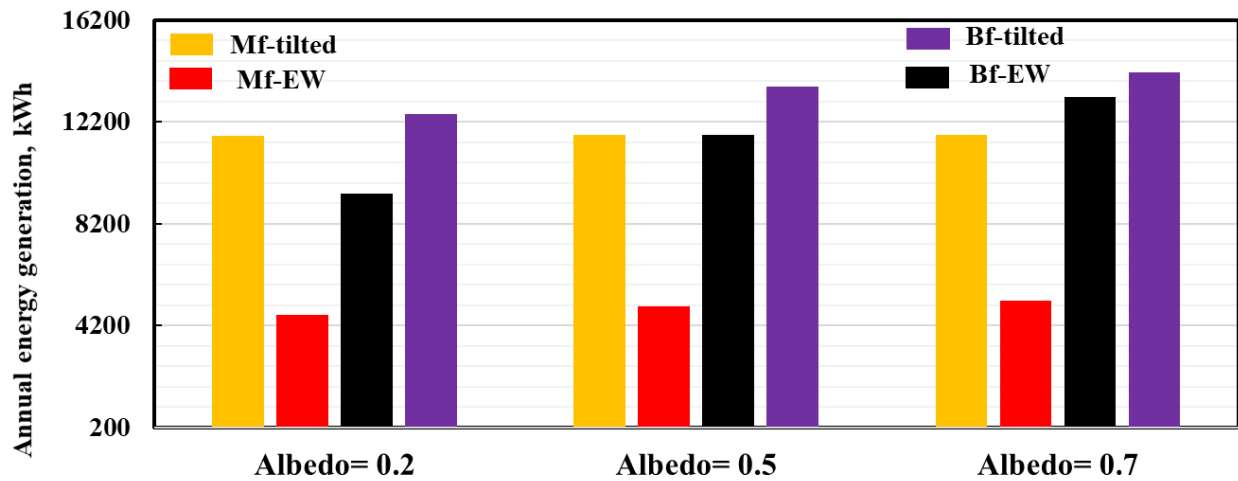


Figure 15: Annual energy yield in kWh for the different PV configurations.

In order to further compare the vertical and tilted bi-facial PVs, the effect of replacing the mono-facial tilted PV with the two types of bi-facial PVs is presented in Table 8. The bi-facial tilted PV

system can generate more energy for the three albedo values than tilted mono-facial PV. The percentage of enhancement increases as albedo increases, as reported in the literature [67-70]. The enhancement of power generation ranged between 7% and 21% for an albedo of 0.2 and 0.7 using tilted bi-facial PV compared to that of tilted mono-facial PV. The enhancement of using a bi-facial vertical PV system is attained only at an albedo value of 0.7. The negative values of the estimated GR represent that the mono-facial tilted PV system is generating more energy compared to the vertical bi-facial PV module at ground albedo of 0.2 and 0.5. At albedo = 0.2, the corresponding enhancement was very close to that obtained by Janssen *et al.* [71], where the location of the study was Amsterdam.

Table 8: Comparison of power gain ratio for bi-facial PV cells at different albedo values.

albedo	<b>Power GR= <math>(P_{\text{bi-facial}} - P_{\text{mono,tilted}}) / (P_{\text{mono,tilted}}) * 100</math> (%)</b>	
	Bi-facial, tilted	Bi-facial, vertical E-W
0.2	7.18	-19.4
0.5	16.16	-0.09
0.7	20.88	12.65

## 5. Conclusions

In this study, a comparison of bi-facial and mono-facial PV cells was carried out under the climatic conditions of Sharjah, UAE. In contrast to previous studies, the effect of the TPT layer was taken into consideration in the present paper. Several parameters were investigated to study their effect on the performance of PV cells, including solar radiation, ambient temperature, wind speed, albedo, TPT layer absorptivity, and orientation. Regardless of all factors and conditions, PV cell temperature and efficiency were always inversely proportional in mono-facial and bi-facial PV cells. The efficiency of both PV cells changes by about 0.065% for every 1°C increase in

temperature. The efficiency of both types of PV cells was negatively impacted by solar radiation and ambient temperature while being positively impacted by wind speed. Compared to mono-facial cells, bi-facial cells were more sensitive to wind speed, although their sensitivity to ambient temperature was similar. In comparison to the situation of neglected absorptivity, the temperature of the optimally tilted mono-facial PV cell rose by 0.4°C, 1°C, and 1.4°C at albedo values of 0.2, 0.5, and 0.7, respectively. If the absorptivity increases, the rise in PV cell temperature will be more significant, which imposes the need to design the rear side precisely, focusing on the value of absorptivity. As albedo increased from 0.2 to 0.7, the percentage of solar radiation received by the rear side increased from 7% to 19% with respect to the total solar radiation received by the entire PV. Thus, the effect of albedo on the received solar radiation was greater on the rear side compared to the front side. Based on the year-long comparison, the tilted bi-facial PV performed better than the vertical E-W bi-facial PV for all values of albedo. The power gain ratio of the tilted bi-facial ranged from 7.18 to 20.88%, while that of vertical bi-facial ranged from -19.4 to 12.65% as the albedo increased from 0.2 to 0.7.

The authors believe that conducting a life cycle assessment along with a cost comparison of the two systems and estimating the LCOE for both PV systems working mono-facial and bi-facial PV modules could be worth to be investigated in the future. Additionally, developing an efficient thermal management method for this type of PV module can be another research trend to be evaluated. Further investigations could be done to study the effect of bi-facial PV modules on each other, considering different orientations. This is important to figure out what the positive and negative parameters are that would help in determining the optimal positioning of solar PVs in power generation plants.



## Acknowledgments

The authors would like to thank Ayman Mdallal for his support in performing the year-long simulation using PVsys.

## References

- [1] S. Mehranfar, A. Gharehghani, A. Azizi, A. Mahmoudzadeh Andwari, A. Pesyridis, and H. Jouhara, "Comparative assessment of innovative methods to improve solar chimney power plant efficiency," *Sustainable Energy Technologies and Assessments*, vol. 49, p. 101807, 2022/02/01/ 2022, doi: <https://doi.org/10.1016/j.seta.2021.101807>.
- [2] A. Bensalah, G. Barakat, and Y. Amara, "Electrical Generators for Large Wind Turbine: Trends and Challenges," *Energies*, vol. 15, no. 18, doi: 10.3390/en15186700.
- [3] M. Mahmoud, M. Ramadan, S. Naher, K. Pullen, M. Ali Abdelkareem, and A.-G. Olabi, "A review of geothermal energy-driven hydrogen production systems," *Thermal Science and Engineering Progress*, vol. 22, p. 100854, 2021/05/01/ 2021, doi: <https://doi.org/10.1016/j.tsep.2021.100854>.
- [4] J. J. Alvarado Flores *et al.*, "Analysis of Pyrolysis Kinetic Parameters Based on Various Mathematical Models for More than Twenty Different Biomasses: A Review," *Energies*, vol. 15, no. 18, doi: 10.3390/en15186524.
- [5] B. Yang *et al.*, "Wave energy converter array layout optimization: A critical and comprehensive overview," *Renewable and Sustainable Energy Reviews*, vol. 167, p. 112668, 2022/10/01/ 2022, doi: <https://doi.org/10.1016/j.rser.2022.112668>.
- [6] M. Thiébaud *et al.*, "Investigating the flow dynamics and turbulence at a tidal-stream energy site in a highly energetic estuary," *Renewable Energy*, vol. 195, pp. 252-262, 2022/08/01/ 2022, doi: <https://doi.org/10.1016/j.renene.2022.06.020>.
- [7] N. F. Yah, A. N. Oumer, and M. S. Idris, "Small scale hydro-power as a source of renewable energy in Malaysia: A review," *Renewable and Sustainable Energy Reviews*, vol. 72, pp. 228-239, 2017/05/01/ 2017, doi: <https://doi.org/10.1016/j.rser.2017.01.068>.
- [8] M. Mahmoud, M. Ramadan, S. Naher, K. Pullen, and A.-G. Olabi, "The impacts of different heating systems on the environment: A review," *Science of The Total Environment*, vol. 766, p. 142625, 2021/04/20/ 2021, doi: <https://doi.org/10.1016/j.scitotenv.2020.142625>.
- [9] H. Jo, Y. Joo, and D. Kim, "Thermal design of solar thermoelectric generator with phase change material for timely and efficient power generation," *Energy*, p. 125604, 2022/10/03/ 2022, doi: <https://doi.org/10.1016/j.energy.2022.125604>.
- [10] S. Chantasiriwan, "Comparison between two solar feed water heating systems in thermal power plant," *International Journal of Thermofluids*, vol. 15, p. 100167, 2022/08/01/ 2022, doi: <https://doi.org/10.1016/j.ijft.2022.100167>.
- [11] W. S. Weerakkody *et al.*, "Carbon capture by macroalgae *Sarcodia suae* using aquaculture wastewater and solar energy for cooling in subtropical regions," *Science of The Total Environment*, vol. 812, p. 152037, 2021/12/01/ 2021, doi: <https://doi.org/10.1016/j.scitotenv.2021.152037>.

- Environment*, vol. 855, p. 158850, 2023/01/10/ 2023, doi: <https://doi.org/10.1016/j.scitotenv.2022.158850>.
- [12] H. M. Maghrabie *et al.*, "A review of solar chimney for natural ventilation of residential and non-residential buildings," *Sustainable Energy Technologies and Assessments*, vol. 52, p. 102082, 2022/08/01/ 2022, doi: <https://doi.org/10.1016/j.seta.2022.102082>.
- [13] A. Gorjian, E. Rahmati, S. Gorjian, A. Anand, and L. D. Jathar, "A comprehensive study of research and development in concentrating solar cookers (CSCs): Design considerations, recent advancements, and economics," *Solar Energy*, vol. 245, pp. 80-107, 2022/10/01/ 2022, doi: <https://doi.org/10.1016/j.solener.2022.08.066>.
- [14] R. Karthikeyan, P. Thangavel, R. T. Raghunath, K. A. Muthu Priyan, and M. Praveen Balaji, "Performance analysis of greenhouse solar dryer using evacuated tubes," *Materials Today: Proceedings*, 2022/07/11/ 2022, doi: <https://doi.org/10.1016/j.matpr.2022.06.447>.
- [15] S. Shoeibi, S. A. A. Mirjalily, H. Kargarsharifabad, M. Khiadani, and H. Panchal, "A comprehensive review on performance improvement of solar desalination with applications of heat pipes," *Desalination*, vol. 540, p. 115983, 2022/10/15/ 2022, doi: <https://doi.org/10.1016/j.desal.2022.115983>.
- [16] K. Obaideen *et al.*, "On the contribution of solar energy to sustainable developments goals: Case study on Mohammed bin Rashid Al Maktoum Solar Park," *International Journal of Thermofluids*, vol. 12, p. 100123, 2021/11/01/ 2021, doi: <https://doi.org/10.1016/j.ijft.2021.100123>.
- [17] A. G. Olabi, M. Mahmoud, B. Soudan, T. Wilberforce, and M. Ramadan, "Geothermal based hybrid energy systems, toward eco-friendly energy approaches," *Renewable Energy*, vol. 147, pp. 2003-2012, 2020/03/01/ 2020, doi: <https://doi.org/10.1016/j.renene.2019.09.140>.
- [18] H. Jouhara, A. Żabnieńska-Góra, N. Khordehghah, D. Ahmad, and T. Lipinski, "Latent thermal energy storage technologies and applications: A review," *International Journal of Thermofluids*, vol. 5-6, p. 100039, 2020/08/01/ 2020, doi: <https://doi.org/10.1016/j.ijft.2020.100039>.
- [19] M. Mahmoud, M. Ramadan, A.-G. Olabi, K. Pullen, and S. Naher, "A review of mechanical energy storage systems combined with wind and solar applications," *Energy Conversion and Management*, vol. 210, p. 112670, 2020/04/15/ 2020, doi: <https://doi.org/10.1016/j.enconman.2020.112670>.
- [20] G. C. d. Andrade Furtado, A. L. Amarante Mesquita, and J. D. Hunt, "Solar Photovoltaic Energy and Pumped Hydro Storage System Coupling in Southern Countries," in *Encyclopedia of Energy Storage*, L. F. Cabeza Ed. Oxford: Elsevier, 2022, pp. 205-213.
- [21] H. Jouhara *et al.*, "Heat pipe based battery thermal management: Evaluating the potential of two novel battery pack integrations," *International Journal of Thermofluids*, vol. 12, p. 100115, 2021/11/01/ 2021, doi: <https://doi.org/10.1016/j.ijft.2021.100115>.
- [22] M. Mahmoud *et al.*, "Phase Change Materials Integrated Into Solar Parabolic Collectors," *Encyclopedia of Smart Materials*, vol. 2, pp. 613-620, 2022/01/01/ 2022, doi: <https://doi.org/10.1016/B978-0-12-815732-9.00084-X>.
- [23] M. Milani *et al.*, "Experimental and numerical analysis of a liquid aluminium injector for an Al-H<sub>2</sub>O based hydrogen production system," *International Journal of Thermofluids*, vol. 7-8, p. 100018, 2020/11/01/ 2020, doi: <https://doi.org/10.1016/j.ijft.2020.100018>.

- [24] A. G. Olabi, Q. Abbas, A. Al Makky, and M. A. Abdelkareem, "Supercapacitors as next generation energy storage devices: Properties and applications," *Energy*, vol. 248, p. 123617, 2022/06/01/ 2022, doi: <https://doi.org/10.1016/j.energy.2022.123617>.
- [25] Y. Zhang, J. Q. Gao, Y. Yu, Q. Shi, and Z. Liu, "Influence of incidence angle effects on the performance of bifacial photovoltaic modules considering rear-side reflection," *Solar Energy*, vol. 245, pp. 404-409, 2022/10/01/ 2022, doi: <https://doi.org/10.1016/j.solener.2022.08.027>.
- [26] T. Hariharasudhan, D. Prince Winston, M. Palpandian, and M. Pravin, "A comparative analysis of polycrystalline and bifacial photovoltaic module under various partial shading condition," *Energy Conversion and Management*, vol. 270, p. 116223, 2022/10/15/ 2022, doi: <https://doi.org/10.1016/j.enconman.2022.116223>.
- [27] G. M. Tina, F. Bontempo Scavo, L. Merlo, and F. Bizzarri, "Analysis of water environment on the performances of floating photovoltaic plants," *Renewable Energy*, vol. 175, pp. 281-295, 2021/09/01/ 2021, doi: <https://doi.org/10.1016/j.renene.2021.04.082>.
- [28] W. Gu, S. Li, X. Liu, Z. Chen, X. Zhang, and T. Ma, "Experimental investigation of the bifacial photovoltaic module under real conditions," *Renewable Energy*, vol. 173, pp. 1111-1122, 2021/08/01/ 2021, doi: <https://doi.org/10.1016/j.renene.2020.12.024>.
- [29] G. M. Tina, F. B. Scavo, S. Aneli, and A. Gagliano, "Assessment of the electrical and thermal performances of building integrated bifacial photovoltaic modules," *Journal of Cleaner Production*, vol. 313, p. 127906, 2021/09/01/ 2021, doi: <https://doi.org/10.1016/j.jclepro.2021.127906>.
- [30] M. Prasad and R. Prasad, "Bifacial vs monofacial grid-connected solar photovoltaic for small islands: A case study of Fiji," *Renewable Energy*, vol. 203, pp. 686-702, 2023/02/01/ 2023, doi: <https://doi.org/10.1016/j.renene.2022.12.068>.
- [31] F. Tahir, A. A. B. Baloch, and S. G. Al-Ghamdi, "Impact of climate change on solar monofacial and bifacial Photovoltaics (PV) potential in Qatar," *Energy Reports*, vol. 8, pp. 518-522, 2022/08/01/ 2022, doi: <https://doi.org/10.1016/j.egy.2022.02.197>.
- [32] K. S. Hayibo, A. Petsiuk, P. Mayville, L. Brown, and J. M. Pearce, "Monofacial vs bifacial solar photovoltaic systems in snowy environments," *Renewable Energy*, vol. 193, pp. 657-668, 2022/06/01/ 2022, doi: <https://doi.org/10.1016/j.renene.2022.05.050>.
- [33] K. Barbosa de Melo, M. Kitayama da Silva, J. Lucas de Souza Silva, T. S. Costa, and M. G. Villalva, "Study of energy improvement with the insertion of bifacial modules and solar trackers in photovoltaic installations in Brazil," *Renewable Energy Focus*, vol. 41, pp. 179-187, 2022/06/01/ 2022, doi: <https://doi.org/10.1016/j.ref.2022.02.005>.
- [34] B. Durusoy, T. Ozden, and B. G. Akinoglu, "Solar irradiation on the rear surface of bifacial solar modules: a modeling approach," *Scientific Reports*, vol. 10, no. 1, pp. 1-10, 2020.
- [35] S. A. Mousavi Maleki, H. Hizam, and C. Gomes, "Estimation of hourly, daily and monthly global solar radiation on inclined surfaces: Models re-visited," *Energies*, vol. 10, no. 1, p. 134, 2017.
- [36] A. Abotaleb and A. Abdallah, "Performance of bifacial-silicon heterojunction modules under desert environment," *Renewable Energy*, vol. 127, pp. 94-101, 2018/11/01/ 2018, doi: <https://doi.org/10.1016/j.renene.2018.04.050>.

- [37] S. Guo, T. M. Walsh, and M. Peters, "Vertically mounted bifacial photovoltaic modules: A global analysis," *Energy*, vol. 61, pp. 447-454, 2013/11/01/ 2013, doi: <https://doi.org/10.1016/j.energy.2013.08.040>.
- [38] J. Appelbaum, "Bifacial photovoltaic panels field," *Renewable Energy*, vol. 85, pp. 338-343, 2016/01/01/ 2016, doi: <https://doi.org/10.1016/j.renene.2015.06.050>.
- [39] F. Johansson, B. E. Gustafsson, B. Stridh, and P. E. Campana, "3D-thermal modelling of a bifacial agrivoltaic system: a photovoltaic module perspective," *Energy Nexus*, vol. 5, p. 100052, 2022/03/16/ 2022, doi: <https://doi.org/10.1016/j.nexus.2022.100052>.
- [40] J. Zhou, Q. Yi, Y. Wang, and Z. Ye, "Temperature distribution of photovoltaic module based on finite element simulation," *Solar Energy*, vol. 111, pp. 97-103, 2015/01/01/ 2015, doi: <https://doi.org/10.1016/j.solener.2014.10.040>.
- [41] A. Radwan, M. Emam, and M. Ahmed, "Chapter 2.15 - Comparative Study of Active and Passive Cooling Techniques for Concentrated Photovoltaic Systems," in *Exergetic, Energetic and Environmental Dimensions*, I. Dincer, C. O. Colpan, and O. Kizilkan Eds.: Academic Press, 2018, pp. 475-505.
- [42] Z. S. Zhou, L. W. Wang, L. Jiang, P. Gao, and R. Z. Wang, "Non-equilibrium sorption performances for composite sorbents of chlorides–ammonia working pairs for refrigeration," *International Journal of Refrigeration*, vol. 65, pp. 60-68, 2016/05/01/ 2016, doi: <https://doi.org/10.1016/j.ijrefrig.2015.11.014>.
- [43] A. Radwan and M. Ahmed, "The influence of microchannel heat sink configurations on the performance of low concentrator photovoltaic systems," *Applied Energy*, vol. 206, pp. 594-611, 2017/11/15/ 2017, doi: <https://doi.org/10.1016/j.apenergy.2017.08.202>.
- [44] Y. A. Cengel, M. A. Boles, and M. Kanoğlu, *Thermodynamics: an engineering approach*. McGraw-hill New York, 2011.
- [45] T. Katsaounis *et al.*, "Performance assessment of bifacial c-Si PV modules through device simulations and outdoor measurements," *Renewable Energy*, vol. 143, pp. 1285-1298, 2019/12/01/ 2019, doi: <https://doi.org/10.1016/j.renene.2019.05.057>.
- [46] M. W. P. E. Lamers *et al.*, "Temperature effects of bifacial modules: Hotter or cooler?," *Solar Energy Materials and Solar Cells*, vol. 185, pp. 192-197, 2018/10/01/ 2018, doi: <https://doi.org/10.1016/j.solmat.2018.05.033>.
- [47] M. Leonardi *et al.*, "The Effects of Module Temperature on the Energy Yield of Bifacial Photovoltaics: Data and Model," *Energies*, vol. 15, no. 1, p. 22, 2021.
- [48] I. Santiago, D. Trillo-Montero, I. M. Moreno-Garcia, V. Pallarés-López, and J. J. Luna-Rodríguez, "Modeling of photovoltaic cell temperature losses: A review and a practice case in South Spain," *Renewable and Sustainable Energy Reviews*, vol. 90, pp. 70-89, 2018/07/01/ 2018, doi: <https://doi.org/10.1016/j.rser.2018.03.054>.
- [49] M. Basher and K. Al-Asadi, "Effect of solar radiation on photovoltaic cell," vol. 3, 07/18 2018.
- [50] A. Karafil, "Temperature and Solar Radiation Effects on Photovoltaic Panel Power," *Journal of New Results in Science*, vol. 5, pp. 48-58, 08/01 2016.
- [51] A. Hussien, A. Eltayesh, and H. M. El-Batsh, "Experimental and numerical investigation for PV cooling by forced convection," *Alexandria Engineering Journal*, 2022/09/21/ 2022, doi: <https://doi.org/10.1016/j.aej.2022.09.006>.

- [52] S. Panda, B. Panda, C. Jena, L. Nanda, and A. Pradhan, "Investigating the similarities and differences between front and back surface cooling for PV panels," *Materials Today: Proceedings*, 2022/09/14/ 2022, doi: <https://doi.org/10.1016/j.matpr.2022.08.424>.
- [53] F. Al-Amri, F. Saeed, and M. A. Mujeebu, "Novel dual-function racking structure for passive cooling of solar PV panels –thermal performance analysis," *Renewable Energy*, vol. 198, pp. 100-113, 2022/10/01/ 2022, doi: <https://doi.org/10.1016/j.renene.2022.08.047>.
- [54] Z. Zapałowicz and W. Zeńczak, "Seawater cooling of PV modules mounted on ships in Świnoujście/Poland harbour," *Heliyon*, vol. 8, no. 8, p. e10078, 2022/08/01/ 2022, doi: <https://doi.org/10.1016/j.heliyon.2022.e10078>.
- [55] M. Sattar, A. Rehman, N. Ahmad, A. Mohammad, A. A. Al Ahmadi, and N. Ullah, "Performance Analysis and Optimization of a Cooling System for Hybrid Solar Panels Based on Climatic Conditions of Islamabad, Pakistan," *Energies*, vol. 15, no. 17, doi: 10.3390/en15176278.
- [56] K. Sornek, W. Goryl, R. Figaj, G. Dąbrowska, and J. Brezdeń, "Development and Tests of the Water Cooling System Dedicated to Photovoltaic Panels," *Energies*, vol. 15, no. 16, doi: 10.3390/en15165884.
- [57] J. Li *et al.*, "Performance evaluation of bifacial PV modules using high thermal conductivity fins," *Solar Energy*, vol. 245, pp. 108-119, 2022/10/01/ 2022, doi: <https://doi.org/10.1016/j.solener.2022.09.017>.
- [58] "LG Electronics LG400N3K-V6 NeON H+ 400 Wp Black I Photovoltaic4all." <https://www.photovoltai4all.de/solarmodule/lg-neon-h-lg400n3k-v6-black> (accessed January 15, 2023).
- [59] "LG Solar LG400Q1C-A6 NeON R 400 Watt I photovoltaics4all." <https://www.photovoltai4all.de/lg-solar-lg400q1c-a6-neon-r> (accessed January 15, 2023).
- [60] "SOFAR SUNNY DEER SERIES USER MANUAL Pdf Download | ManualsLib." <https://www.manualslib.com/manual/1298376/Sofar-Sunny-Deer-Series.html> (accessed January 15, 2023).
- [61] R. Kopecek and J. Libal, "Bifacial photovoltaics 2021: Status, opportunities and challenges," *Energies*, vol. 14, no. 8, p. 2076, 2021.
- [62] A. A. B. Baloch, S. Hammat, B. Figgis, F. H. Alharbi, and N. Tabet, "In-field characterization of key performance parameters for bifacial photovoltaic installation in a desert climate," *Renewable Energy*, vol. 159, pp. 50-63, 2020/10/01/ 2020, doi: <https://doi.org/10.1016/j.renene.2020.05.174>.
- [63] R. Shigenobu, M. Ito, and H. Taoka, "Optimal design of bifacial PV system to mitigate duck-curve problem of power system with the UC problem," *Energy Reports*, vol. 7, pp. 7004-7014, 2021/11/01/ 2021, doi: <https://doi.org/10.1016/j.egy.2021.10.060>.
- [64] R. Kopecek and J. Libal, "Towards large-scale deployment of bifacial photovoltaics," *Nature Energy*, vol. 3, no. 6, pp. 443-446, 2018.
- [65] W. Gu, T. Ma, M. Li, L. Shen, and Y. Zhang, "A coupled optical-electrical-thermal model of the bifacial photovoltaic module," *Applied Energy*, vol. 258, p. 114075, 2020/01/15/ 2020, doi: <https://doi.org/10.1016/j.apenergy.2019.114075>.

- [66] P. K. Sahu, J. N. Roy, C. Chakraborty, and S. Sundaram, "A New Model for Estimation of Energy Extraction from Bifacial Photovoltaic Modules," *Energies*, vol. 14, no. 16, p. 5089, 2021.
- [67] U. A. Yusufoglu *et al.*, "Simulation of Energy Production by Bifacial Modules with Revision of Ground Reflection," *Energy Procedia*, vol. 55, pp. 389-395, 2014/01/01/ 2014, doi: <https://doi.org/10.1016/j.egypro.2014.08.111>.
- [68] V. Durković and Ž. Đurišić, "Extended model for irradiation suitable for large bifacial PV power plants," *Solar Energy*, vol. 191, pp. 272-290, 2019/10/01/ 2019, doi: <https://doi.org/10.1016/j.solener.2019.08.064>.
- [69] I. Shoukry, J. Libal, R. Kopecek, E. Wefringhaus, and J. Werner, "Modelling of Bifacial Gain for Stand-alone and in-field Installed Bifacial PV Modules," *Energy Procedia*, vol. 92, pp. 600-608, 2016/08/01/ 2016, doi: <https://doi.org/10.1016/j.egypro.2016.07.025>.
- [70] R. Satpathy, "Additional energy yield using bifacial solar PV modules & dependency on Albedo," *Jakson, Empowering People*, [Consulta 5 enero del 2020]. Disponible en <https://www.ises.org>.
- [71] G. J. M. Janssen, B. B. Van Aken, A. J. Carr, and A. A. Mewe, "Outdoor Performance of Bifacial Modules by Measurements and Modelling," *Energy Procedia*, vol. 77, pp. 364-373, 2015/08/01/ 2015, doi: <https://doi.org/10.1016/j.egypro.2015.07.051>.